iScience

CellPress

Article

PTPRA Phosphatase Regulates GDNF-Dependent RET Signaling and Inhibits the RET Mutant MEN2A Oncogenic Potential

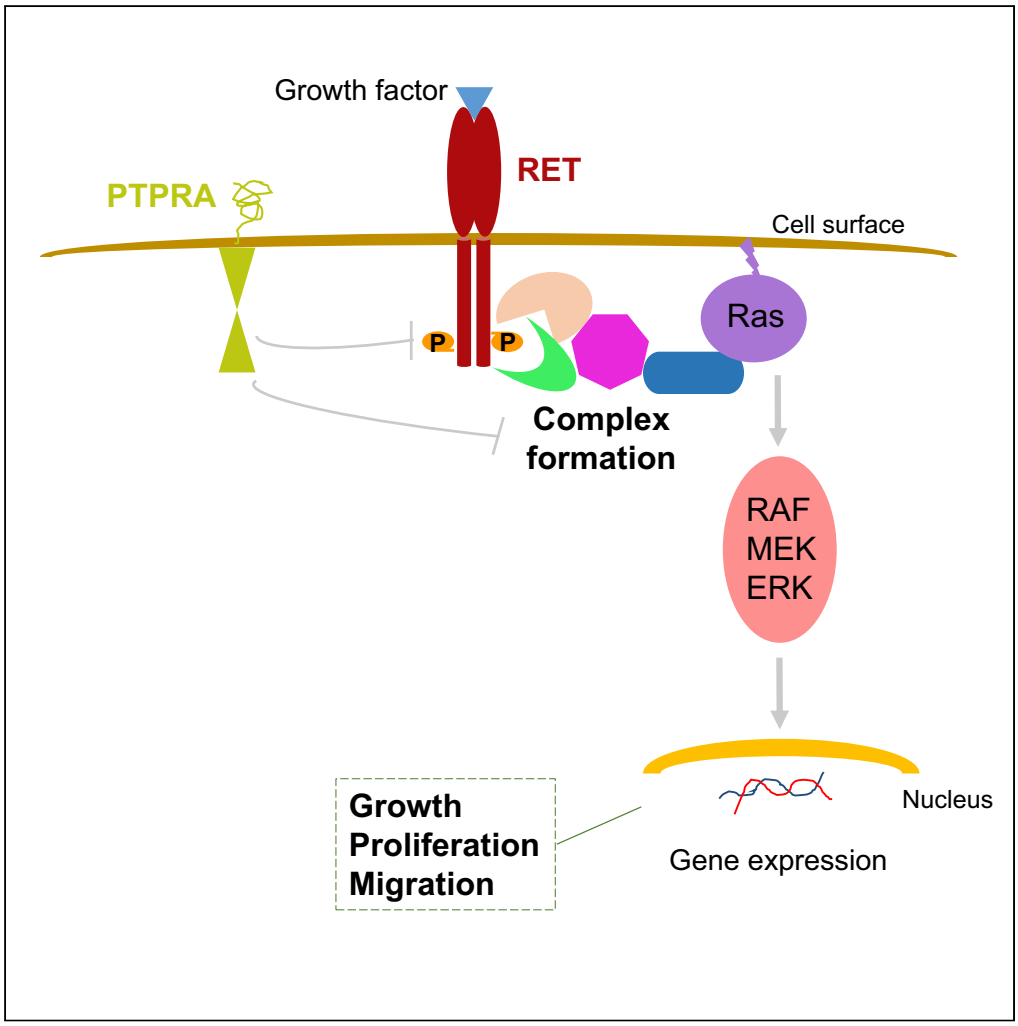

Leena Yadav, Elina Pietilä, Tiina Öhman, ..., Kaisa Lehti, Mart Saarma, Markku Varjosalo

markku.varjosalo@helsinki.fi

HIGHLIGHTS

PTPRA inhibits ligand (GDNF-GFRα1)-mediated RET activity on Ras-MAPK signaling axis

PTPRA dephosphorylate RET on key functional phosphotyrosine sites

PTPRA catalytic (PTPase) domain 1 regulates RET-driven signaling

PTPRA suppresses RET oncogenic mutant MEN2A in both Ras-MAPK and cell invasion models

Yadav et al., iScience *23*, 100871
February 21, 2020
https://doi.org/10.1016/j.isci.2020.100871

iScience

CellPress

Article

PTPRA Phosphatase Regulates GDNF-Dependent RET Signaling and Inhibits the RET Mutant MEN2A Oncogenic Potential

Leena Yadav,[1] Elina Pietilä,[3,5] Tiina Öhman,[1,5] Xiaonan Liu,[1] Arun K. Mahato,[2] Yulia Sidorova,[2] Kaisa Lehti,[3,4] Mart Saarma,[2] and Markku Varjosalo[1,6,*]

SUMMARY

The RET proto-oncogene encodes receptor tyrosine kinase, expressed primarily in tissues of neural crest origin. De-regulation of RET signaling is implicated in several human cancers. Recent phosphatome interactome analysis identified PTPRA interacting with the neurotrophic factor (GDNF)-dependent RET-Ras-MAPK signaling-axis. Here, by identifying comprehensive interactomes of PTPRA and RET, we reveal their close physical and functional association. The PTPRA directly interacts with RET, and using the phosphoproteomic approach, we identify RET as a direct dephosphorylation substrate of PTPRA both *in vivo* and *in vitro*. The protein phosphatase domain-1 is indispensable for the PTPRA inhibitory role on RET activity and downstream Ras-MAPK signaling, whereas domain-2 has only minor effect. Furthermore, PTPRA also regulates the RET oncogenic mutant variant MEN2A activity and invasion capacity, whereas the MEN2B is insensitive to PTPRA. In sum, we discern PTPRA as a novel regulator of RET signaling in both health and cancer.

INTRODUCTION

Protein tyrosine phosphorylation is a prime eukaryotic regulatory step for intracellular signal transduction and is maintained by opposing activities of protein tyrosine kinases (PTKs) and phosphatases (PTPs). Strikingly, the number of PTPs (107) encoded by the human genome roughly matches that of PTKs (90), indicating that PTPs might also have equivalent functional complexity and specificity as their kinase counterparts. However, unlike PTKs, biological circuitry and activity control mechanisms of many PTPs are still undefined. Recently, through global systematic interactome analysis of human protein phosphatases, we have demonstrated that GDNF (glial cell line-derived neurotrophic factor) and GRB2 (growth factor receptor-bound protein 2) form a complex with the protein tyrosine phosphatase receptor-type A (PTPRA) (Yadav et al., 2017). To our interest, GDNF acts as a key homodimeric neurotrophic factor family ligand, which in conjunction with GDNF α-receptors (GFRα1-4; glycosylphosphatidylinositol-anchored proteins) incite RET (REarranged during Transfection) receptor tyrosine kinase via dimerization to prompt Ras-MAPK (mitogen-activated protein kinase) cascade and other signaling pathways (Airaksinen and Saarma, 2002; Arighi et al., 2005). Notably, only a few protein phosphatases such as PTPRF (Leukocyte common antigen-related; LAR), PTN6 (Src homology region 2 domain-containing phosphatase-1; SHP1), and PTN11 (Src homology region 2 domain-containing phosphatase-2; SHP2) have been suggested to balance the phosphorylation and oncogenic activity of RET (Hennige et al., 2001; Perrinjaquet et al., 2010; Qiao et al., 2001).

Similar to PTPRF, PTPRA is a membrane-bound "receptor-type" protein tyrosine phosphatase, with a highly glycosylated ectodomain, a single membrane-spanning region, and two intracellular catalytic phosphatase domains (PTPase; membrane-proximal D1 and -distal D2) (Daum et al., 1994; Wang and Pallen, 1991; Wu et al., 1997). Although ubiquitously expressed, it is particularly abundant in the brain (neurons and glial cells) and insulin target tissues, where it induces cell differentiation, migration, activation of voltage-gated potassium channels, and insulin secretion (Chen et al., 2009; Imbrici et al., 2000; Kaplan et al., 1990; Kapp et al., 2003; Norris et al., 1997; Petrone et al., 2003). Nevertheless, several previous studies have disclosed its critical role as a main positive regulator of Src family kinases (Fyn, FAK, and Src) in cell growth and oncogenic transformation (Huang et al., 2011; Tremper-Wells et al., 2010; Zheng et al., 2002). Conforming with this, PTPRA has been suggested to play a dual role in regulating EGFR kinase signaling via Src dephosphorylation and activation (Yao et al., 2017). Despite these findings, relatively few signaling pathways (cell

[1]Systems Biology/Pathology Research Group and Proteomics Unit, Institute of Biotechnology, HiLIFE, University of Helsinki, Helsinki 00014, Finland

[2]Laboratory of Molecular Neuroscience, Institute of Biotechnology, HiLIFE, University of Helsinki, Helsinki 00014, Finland

[3]Research Programs Unit, Individualized Drug Therapy, Biomedicum, University of Helsinki and Helsinki University Hospital, Helsinki 00014, Finland

[4]Department of Microbiology, Tumor and Cell Biology (MTC), Karolinska Institutet, Stockholm 17177, Sweden

[5]These authors contributed equally

[6]Lead Contact

*Correspondence: markku.varjosalo@helsinki.fi

https://doi.org/10.1016/j.isci.2020.100871

adhesion- and integrin-mediated processes) and cellular targets (or substrates) have been suggested that could unravel the PTPRA-mediated regulation of cellular signaling (Bodrikov et al., 2005; Truffi et al., 2014; Yao et al., 2017).

In addition to the matching cellular localization, the RET and PTPRA tissue expression also coincide. RET is distinctly expressed in neural tissues (brain and enteric nervous system) and in the developing kidney, where it instigates axonal guidance, neuronal survival, and ureteric bud morphogenesis (Pachnis et al., 1993). Its malfunctioning is described in neuroendocrine tumors and diseases (neurocristopathies) such as renal cell carcinoma, multiple endocrine neoplasia type 2 (MEN2), neuroblastoma, and Parkinson's disease (Drinkut et al., 2016; Mulligan, 2014; Schedl, 2007). For example, in MEN2 syndrome, RET carries numerous gain-of-function mutations in extracellular (C634W; MEN2A) and catalytic (M918T; MEN2B) domains, which leads to aberrant kinase activation and, eventually, to pheochromocytomas and medullary thyroid carcinomas (Eng and Mulligan, 1997; Santoro et al., 2004). Importantly, GDNF-GFRα1-activated RET is autophosphorylated at discrete intracellular tyrosine-sites, Y981, Y1015, Y1062, and Y1096 (Y1096 found only in RET51 isoform), which provide docking sites for downstream adaptors or effectors (Src, SHC, GRB2, Enigma, and DOK proteins) and coordinate four key signaling routes: Ras-MAPK, PI3K-AKT, Src, and PLC-γ pathways (Amoresano et al., 2005; Besset et al., 2000; Coulpier et al., 2002; Goodman et al., 2014; Melillo et al., 2001). Among these sites, autophosphorylation of Y1062 is critical for the initiation of Ras-MAPK (GRB2-SOS complex) and PI3K-AKT (GRB2-GAB1 complex) relays in response to GDNF-GFRα1 co-complex during neuronal survival and proliferation (Besset et al., 2000; Coulpier et al., 2002; Kawamoto et al., 2004).

To decipher the GDNF-GFRα1-mediated RET-Ras-MAPK signaling-axis regulation by PTPRA, we mapped in-depth molecular interactions and mechanisms involved. Additionally, we focused on the plausible anticancer function of PTPRA and, especially, on its role in the regulation of the two oncogenic RET mutants MEN2A (C634W) and MEN2B (M918T) in cancer cessation. The possibility to modulate the oncogenic effects of MEN2A or MEN2B via regulating PTPRA activity would be intriguing and could likely offer novel therapeutic avenues for treating MEN2-type tumors.

RESULTS AND DISCUSSION

Structural-Functional Coherence of PTPRA and RET Complexes

To expand the analysis of the functional cross talk between PTPRA and the GDNF-induced RET signaling, we applied both affinity purification-mass spectrometry (AP-MS) and proximity-dependent biotin identification (BioID) interaction proteomic approaches, now, using GDNF, RET, and GRB2 as bait proteins (Liu et al., 2018; Yadav et al., 2017). The AP-MS allows purification of the intact protein complexes and estimation of their stoichiometry, whereas the BioID enables capturing of extremely transient and close-by interactions (Figure 1A). Hence, for analysis, GDNF, RET, and GRB2 were subcloned into StrepIII-HA and BioID vectors, their corresponding stable, transient, and close-proximity interactors were purified using Strep-Tactin resin, and the interactors were identified with liquid chromatography-mass spectrometry (LC-MS) (Figure 1A) (Liu et al., 2018; Yadav et al., 2017).

Interestingly, the PTPRA and RET interactomes shared many core proteins that operate in various cell growth events (Figure 1B and Table S1). For example, Ras-MAPK pathway commencing cell-surface receptors (IGF1R, TGFR1, EGFR, and ERBB2), intracellular *bona fide* docking proteins (SOS1, SOS2, Src, SHB, SHC1, GAB1, GRB2, and FRS2), and other regulators (MARK3, CRK, and MERL) were identified not only in complex with RET but also with PTPRA (Figure 1B). More so, through extended AP-MS analysis of GRB2, as well as of GDNF, we confirmed GDNF-RET, GRB2-PTPRA, and GRB2-SHC1-SOS1-SOS2 associations (Table S1). Consistent with these results, previous studies have described that GDNF-activated RET promotes Ras-MAPK activation, which is essential for development of nervous system (enteric and brain), spermatogenesis, and kidney during embryogenesis (Costantini and Shakya, 2006; Li et al., 2006; Soba et al., 2015; Xiao et al., 2015). Noticeably, we have also retrieved PTPRA interaction with other receptor tyrosine kinases (RTKs) EGFR and ERBB2 (Figure 1B and Table S1), where PTPRA was earlier shown to dephosphorylate EGFR and subject a positive effect on downstream Ras-MAPK signaling through Src activation (Yao et al., 2017). Therefore, we sought to check the specificity of the derived PTPRA and RET interactomes by comparing them with that of EGFR and ERBB2 along with IGF1R kinase, related to RET in neural oncogenesis (Denardo et al., 2013). For this purpose, both AP-MS and BioID approaches were applied to draw the proteomes of these RTKs: EGFR (219 interactions), ERBB2 (111 interactions), and IGF1R (209

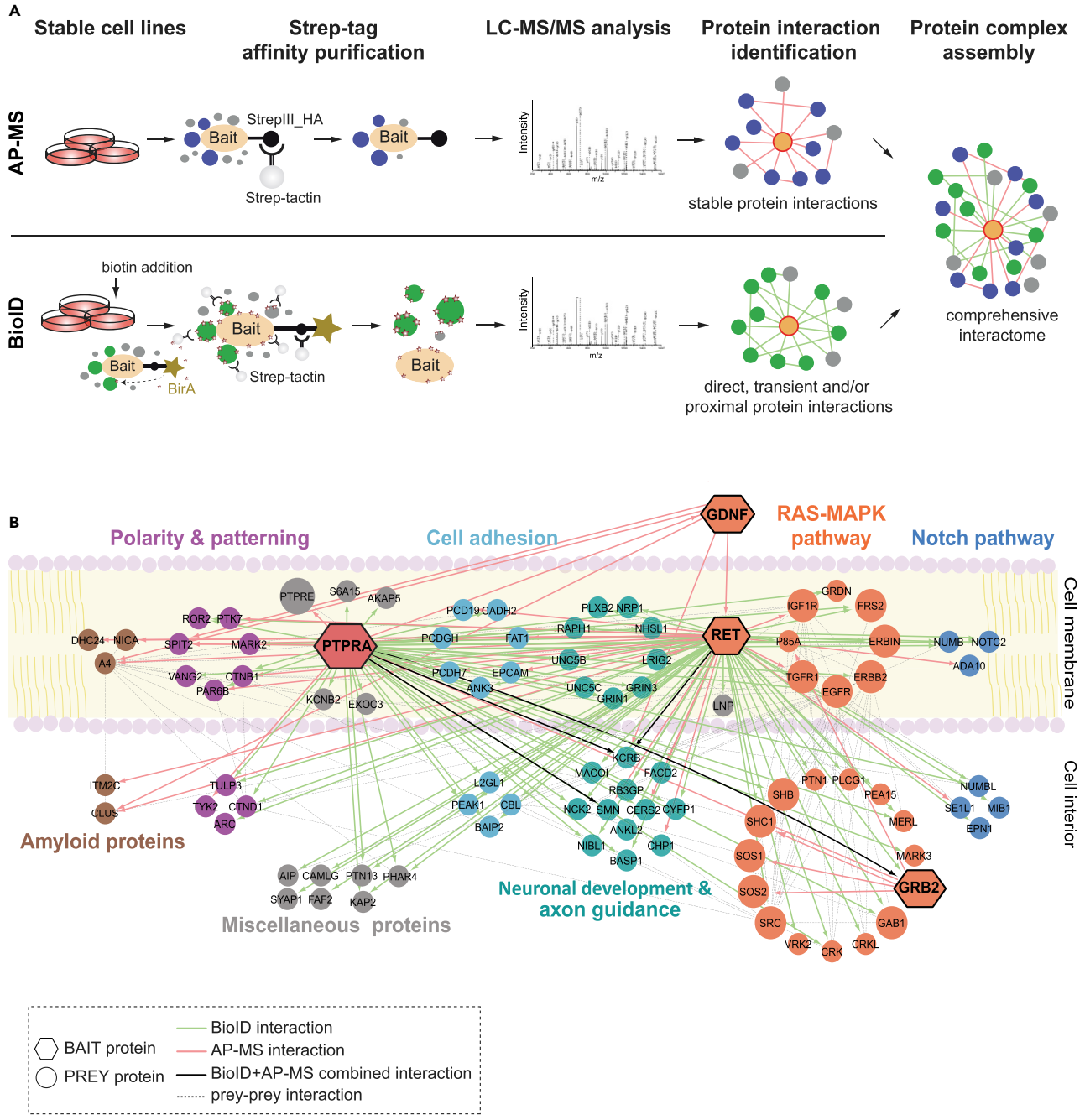

Figure 1. Affinity Purification and Proximity-Dependent Labeling Mass Spectrometry Reveal the Overlap between PTPRA and RET Interactomes

(A) The stable Flp-In-T-REx 293 cells are generated for expression of StrepIII-HA- (AP-MS) and MAC- (BioID) tagged bait proteins (PTPRA, RET, GDNF, and GRB2). The bait expression is induced with tetracycline (AP-MS and BioID baits), and extra biotin is added for BioID baits. Next, the bait complexes are single-step affinity purified and the interacting proteins are identified with LC-MS/MS (n = 4 replicates).

(B) The AP-MS and BioID derived composite protein interaction map of PTPRA and RET as well as GDNF and GRB2 baits (hexagons). Various prey proteins (circles) are grouped based on their biological functions and color coded. Uniprot entry names are used for protein nomenclature. Key: bait-prey interactions (green = BioID; red = AP-MS; and black = both).

See also Figure S1 and Table S1.

interactions) (Salokas et al., Unpublished Data). Upon comparison, PTPRA exhibited <15% common interactions with these RTKs, whereas with RET it shared nearly 49% interactions (Figure S1A and Table S1). Nevertheless, within the Ras-MAPK module, ~7.3 (average) interactions reoccurred in EGFR, ERBB2, and IGF1R proteomes (Figure S1B). Intriguingly, RET interactome also differed substantially from these RTKs with a similarity of about 11% with EGFR, 5% with ERBB2, and 10% with IGF1R, suggesting their characteristic signaling complexes (Figure S1C). Hence, this comparative analysis data not only verified the distinctiveness of our PTPRA and RET interactomes but also indicated cross talk of PTPRA in regulating RET-mediated Ras-MAPK signaling, by virtue of their converging interaction frameworks (PTPRA-EGFR-FRS2-GRB2-GAB1 and RET-FRS2-GRB2-GAB1-SHC1) (Figure 1B and Table S1).

Additionally, overlap of the PTPRA and RET interactomes was also detected with a large cohort of proteins such as UCN5(B-C), NRP1, BASP1, CERS2, VANG2, MARK2, and TULP3, linked to varied aspects of neuronal development, axon guidance, pathfinding, neuronal polarization, and pattern (axis) formation (Figure 1B and Table S1) (Chen et al., 2006; Imgrund et al., 2009; Larrivee et al., 2007; Mosevitsky, 2005; Norman et al., 2009; Poliak et al., 2015; Telley et al., 2016; Torban et al., 2004). Although many of these biological functions are linked to RET, much less is known about PTPRA in regulating these processes. Moreover, the gene expression pattern of PTPRA shows its high levels in the neuroendocrine tissues of the nervous system, kidney, thyroid, and pituitary gland, along with the tumors derived from these tissues (Figure S2). These include astrocytoma, glioblastoma (GBM), oligodendroglioma, mixed glioma, nephroblastoma, and thyroid carcinoma, further implicating the importance of PTPRA in neural development (Figure S2). Therefore, collectively, as our proteomic results point toward physical and functional interaction between PTPRA and RET, we set out to study if RET activity would be PTPRA regulated and if RET would be a direct substrate of PTPRA.

PTPRA Inhibits the RET-Ras-MAPK Signaling Pathway

The activation of RET by GDNF-GFRα1 complex is the first event in the activation of the Ras-MAPK signaling and acts as a catalyst for the downstream relay. Therefore, to determine the effect of PTPRA on this pathway, we developed a RET-Ras-MAPK activation detection system in HEK293 cells, which included StrepIII-HA-tagged RET (RET9), Elk1-Gal4-binding domain (GBD) effector (pGBD-Elk1), and Gal4-activation domain (GAD) containing Firefly luciferase (pGAD-FR-Luc) reporter along with Renilla luciferase (phR-Luc) control reporter (Figure 2A). Upon activation by GDNF-GFRα1, the reporter system shows >5-fold pathway activity induction. Since HEK293 cells exhibit undetectable levels of endogenously expressed PTPRA (https://amp.pharm.mssm.edu 〉 Harmonizome and Geiger et al., 2012), this system was then used for assessing the outcomes of transfecting increasing amounts of PTPRA (0, 10, 25, and 50 ng), alongside GFP control, on the RET-Ras-MAPK pathway activity in the presence or absence of soluble GDNF-GFRα1 (100–500 ng/mL; 24 h) ligand complex (Figure 2B). The maximal inhibition on the ligand-activated pathway (orange bar) was achieved with transfection of 50 ng PTPRA (~2-fold, $p = 0.0001$) (Figure 2B). Notably, the basal pathway activity (blue bar) was also restricted to a similar extent (~1.5-fold) (Figure 2B). The detected inhibitory role of PTPRA in RET-Ras-MAPK cascade was further verified using MG87RET reporter fibroblast cells stably expressing RET (Eketjall et al., 1999). Even under steady RET levels, the PTPRA expression moderated (1.9- to 2.4-fold) the MAPK activation to nearly comparable extents (Figure 2C). This not only validated the attained HEK293 luciferase-reporter assay results but also affirmed the reliability and usability of the RET-Ras-MAPK activation detection system in transiently transfected HEK293 cells.

PTPRA Impacts Downstream RET-Ras-MAPK Signaling

We then followed up the ramification of PTPRA expression on subsequent signaling target MAPKs (ERK1 and ERK2). To do so, HEK293-MSR cell lysates, containing RET (StrepIII-HA-tagged) and increasing amounts of wild-type PTPRA (V5-tagged), were prepared in the absence and presence (15 min stimulation) of GDNF-GFRα1 ligands. The immunoblotting with site-specific p44/42 MAPK (T202/Y204) antibody shows that the phosphorylation of endogenous ERKs (1 and 2) was readily induced by the ligand-activated RET and expression of PTPRA potentiated their phosphorylation, which concluded the PTPRA-facilitated RET-Ras-MAPK inhibition (Figure 3A).

Furthermore, from PTPRA and RET complex analysis, we have observed their strong interaction with GRB2, an adaptor signaling protein (Table S1). Previously, GRB2, in complex with other docking (adaptor) proteins including Src kinase, has been reported to bind RET and harmonize the Ras-MAPK cascade (Alberti et al., 1998; Ohiwa et al., 1997), whereas PTPRA could sequester the SH2 domain of not only GRB2 but also of Src

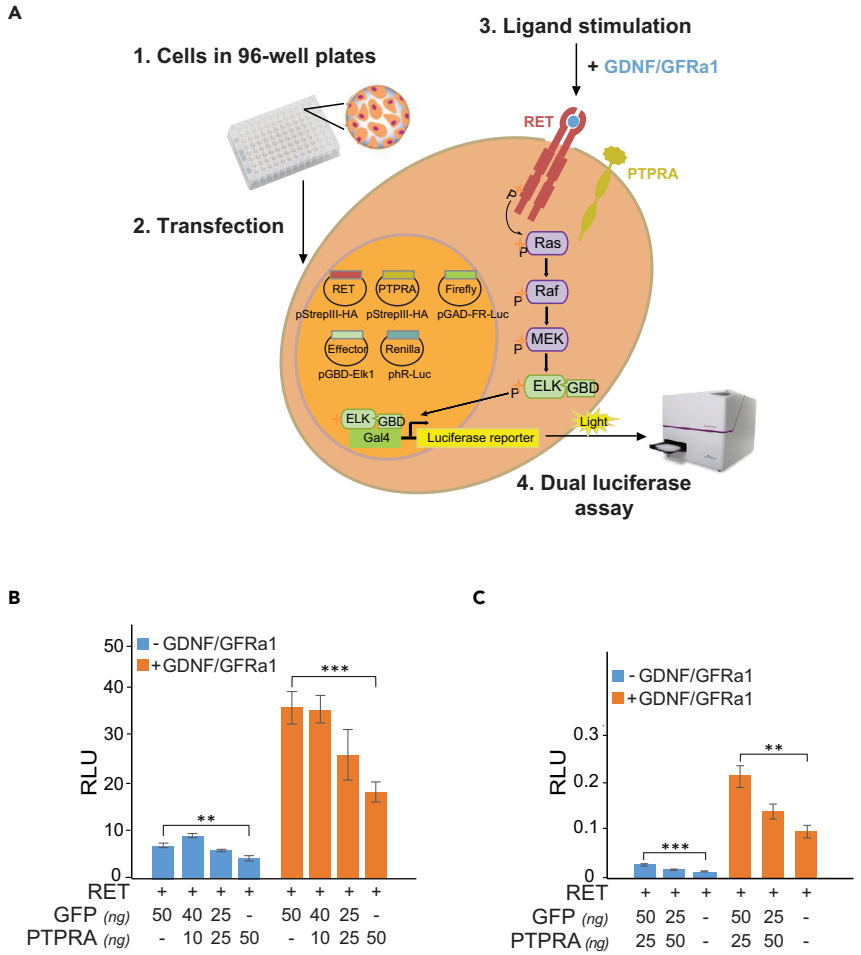

Figure 2. RET-Ras-MAPK Dual-Luciferase Reporter System

(A) HEK293 cells in 96-well plate format are transiently transfected with RET (StrepIII-HA C-terminal tag) and Gal4-binding domain-containing Elk1 (pGBD-Elk1) together with Firefly Gal4-activation domain-containing luciferase (pGAD-FR-Luc), transfection control Renilla luciferase (hR-Luc), PTPRA (StrepIII-HA), and GFP control (StrepIII-HA) expression vectors. GDNF (100 ng/mL) and GFRα1 (500 ng/mL) co-complex is added for 24 h to induce the RET-Ras-MAPK pathway activation. Then, the cells are rapidly lysed and the dual-luciferase signal is measured with a luminometer. The Firefly luciferase values are normalized by the transfection control Renilla luciferase signal values to obtain relative luciferase signal (RLU). (B and C) (B) HEK293 and (C) MG87RET cells expressing RET, transiently (B) or stably (C), show decreased RET-Ras-MAPK pathway activity with increasing amounts (0, 10, 25, 50 ng) of PTPRA alongside GFP control (50, 25, 40, 0 ng) in absence (blue bars) and presence (orange bars) of GDNF-GFRα1 ligands. The bar graph is representative of two independent experiments, where all bars indicate average ratios (n = 5 replicates) of Firefly to Renilla luciferase counts (relative luciferase unit, RLU) and the error bars designate one standard deviation. The statistical significance is obtained by a two-tailed Student's t test (***$p < 0.0001$ and **$p < 0.001$).

through its phosphorylated Y789 site, thereby, linking PTPRA to other key components of cellular signaling (Den Hertog et al., 1994; Denhertog and Hunter, 1996; Zheng et al., 2000). Apparently, in our proteomic analysis, we spotted RET-Src interaction, but with low overall interaction strength, whereas PTPRA-Src interaction was not retrieved (Table S1). Hence, we tested the role of GRB2 in PTPRA-induced RET-Ras-MAPK down-regulation by creating PTPRA Y789F (tyrosine; Y to phenylalanine; F) mutation (Figure 4A). We carried out co-immunoprecipitation of either wild-type PTPRA or Y789F mutant (StrepIII-HA-tagged) with GRB2 (V5-tagged). As shown in Figure 3B, the PTPRA-GRB2 interaction was fully abolished and slightly higher phosphorylation of MAPKs (ERK1 and ERK2) was obtained with Y789F mutant. Then, in Ras-MAPK luciferase assays, PTPRA Y789F mutant competently reduced (~1.63-fold; $p = 2.68 \times 10^{-5}$) the activated RET-Ras-MAPK reporter signal, despite being less active (~1.51-fold; $p = 4.95 \times 10^{-4}$) than wild-type

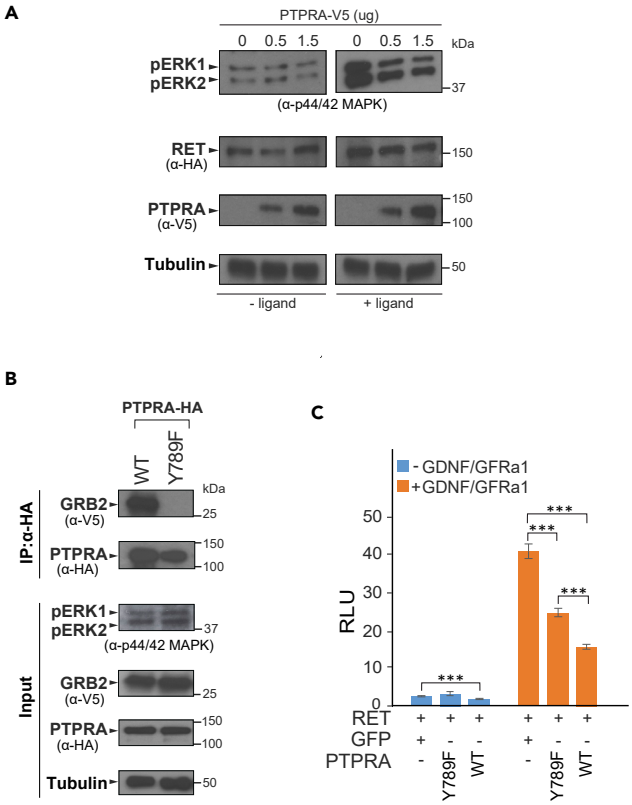

Figure 3. PTPRA Impedes Downstream MAPK (ERK1 and ERK2) Activation and Requires GRB2 for Regulating RET-Ras-MAPK Signaling

(A) HEK293-MSR are co-transfected with RET (StrepIII-HA-tagged) and increasing amounts of V5-tagged PTPRA (0, 0.5, and 1.5 μg) construct. After 15 min stimulation with GDNF-GFRα1 ligands (100–500 ng/mL), the cell lysates were immunoblotted with p44/42 MAPK (T202/Y204) antibody to detect endogenous ERK1 and ERK2 phosphorylation status. Both ERK1 and 2 were dephosphorylated by PTPRA. RET and PTPRA protein expression are determined by anti-HA and anti-V5 antibodies, respectively. Tubulin is used as a loading control.

(B) Either StrepIII-HA-tagged wild-type (WT) PTPRA or Y789F mutant along with V5-tagged GRB2 expression vectors are transiently co-transfected in HEK293-MSR cells. The GRB2 co-immunoprecipitate with WT PTPRA only. The immunoprecipitated (IP) proteins, as well as cell lysates, were immunoblotted with anti-V5 and anti-HA antibodies to detect GRB2 and PTPRA proteins, respectively. The phosphorylation of ERK1 and ERK2 proteins from cell lysate was detected with p44/42 MAPK (T202/Y204) antibody. Tubulin is used as a loading control.

(C) PTPRA Y789F mutant displays significantly decreased phosphatase activity in comparison with WT PTPRA. However, the YF mutant still inhibited RET activity in the Ras-MAPK luciferase-reporter assays, shown in the absence (blue bars) and presence (orange bars) of GDNF-GFRα1 stimulation (100–500 ng/mL; 24 h). The data represent average ratios (n = 5 replicates) of the relative luciferase unit (RLU), and the error bars indicate one standard deviation. The statistical significance is obtained by a two-tailed Student's t test (***$p < 0.0001$).

PTPRA, confirming that Y789 phosphorylation not only is essential for PTPRA-GRB2 interaction but also has direct influence on RET signaling (Figure 3C).

Molecular Determinants of PTPRA-RET Interaction

To investigate the mechanism of PTPRA imposed constraints on RET-Ras-MAPK signaling, we tested how stable or transient the probable direct interaction between PTPRA and RET is and which PTPRA domains are required for its functions. Therefore, we constructed PTPRA membrane-proximal and membrane-distal PTPase D1 and D2 domain deletion (DD; ΔD1 and ΔD2) mutants, respectively (Figure 4A). In particular, both DD mutants retain the juxtamembrane region (JM) involved in protein-protein interactions, as well as the C-terminal tail containing GRB2- and Src-binding sites (Figure 4A). After validating the analogous intracellular localization of these DD mutants with that of wild-type PTPRA, we performed co-immunoprecipitation from HEK293-MSR cells co-expressing either wild-type or DD mutants of PTPRA

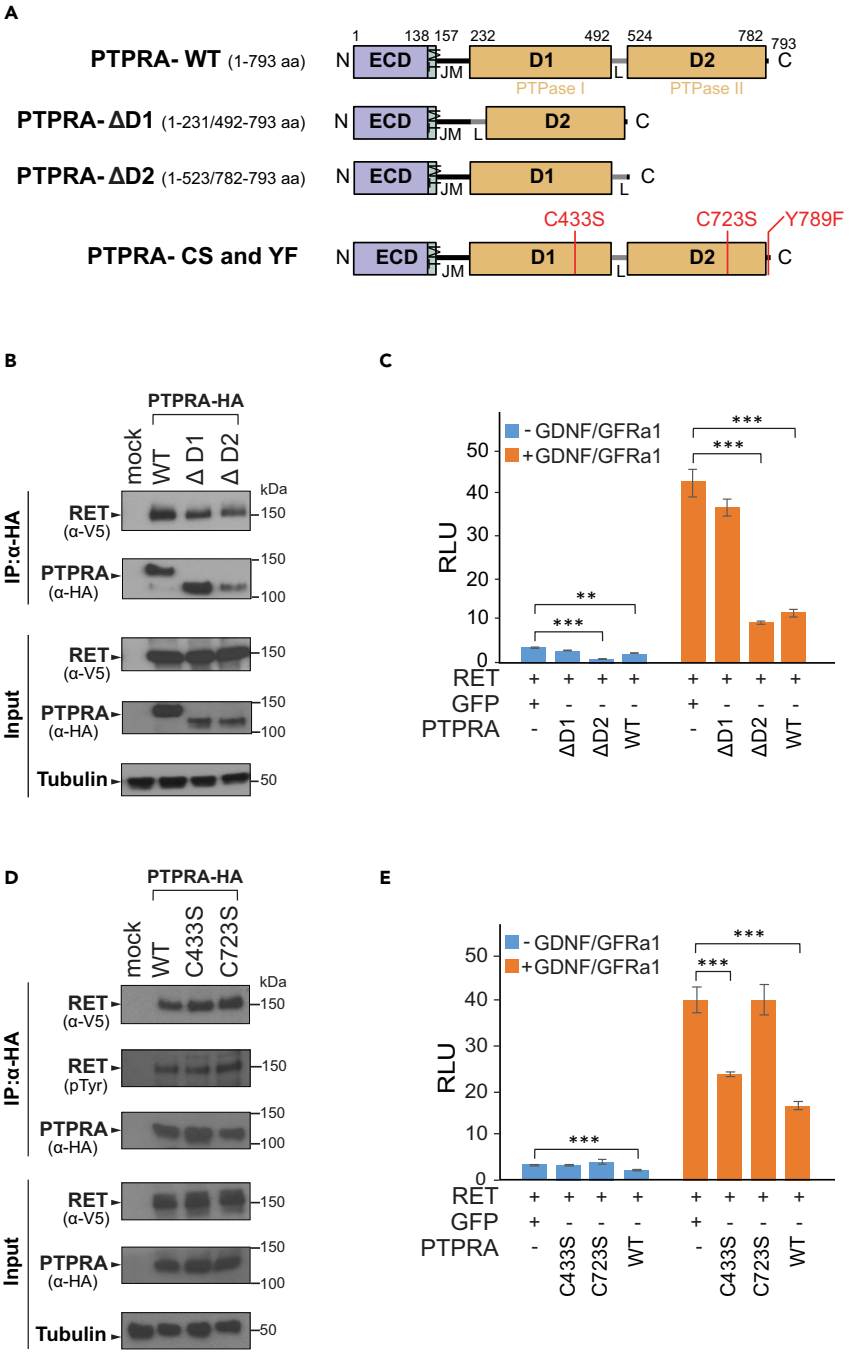

Figure 4. The Activity of PTPase Domain 1 (D1) Is Indispensable for PTPRA-Mediated Negative Regulation of RET

(A) Schematic representation of wild-type (WT) PTPRA and the domain deletion (DD) mutants. The WT PTPRA is a 793 amino acid (aa) long protein. The ΔD1 (1–231/492–793 aa) and ΔD2 (1–523/782–793 aa) correspond to deletions of PTPase I and PTPase II domains, respectively. The catalytic cysteine-to-serine inactivation mutations C433S and C723S in PTPas domain D1 and D2, respectively, along with C-terminal Y789F mutation are indicted as vertical red bars. N, N-terminal; ECD, extracellular domain; TM, transmembrane region; JM, juxtamembrane region; D1, protein tyrosine phosphatase domain 1 (PTPase I); L, interdomain linker region; D2, protein tyrosine phosphatase domain 2 (PTPase II); C, C-terminal tail. See also Figure S3.

(B) HEK293-MSR cells are transiently transfected with either StrepIII-HA-tagged wild-type (WT) PTPRA or DD mutants (ΔD1and ΔD2) along with V5-tagged RET expression vectors. The RET co-precipitates with all the tested PTPRA

Figure 4. *Continued*

constructs. The immunoprecipitated (IP) proteins, as well as cell lysates, were immunoblotted with anti-V5 and anti-HA antibodies to detect RET and PTPRA proteins, respectively. Tubulin is used as a loading control. See also Figure S3.

(C) PTPRA D1 domain deletion mutant ΔD1 displays significant loss of phosphatase activity, whereas both WT and ΔD2 constructs potently inhibit the RET activity in the Ras-MAPK luciferase-reporter assays. The RET-Ras-MAPK pathway activity is shown in the absence (blue bars) and presence (orange bars) of GDNF-GFRα1 co-complex stimulation (100-500 ng/mL; 24 h). The bar graph is representative of two independent experiments, where all bars indicate average ratios (n = 5 replicates) of Firefly to Renilla luciferase counts (relative luciferase unit, RLU) and the error bars designate one standard deviation. The statistical significance is obtained by a two-tailed Student's t test (***$p < 0.0001$ and **$p < 0.001$).

(D) HEK293-MSR cells are transiently transfected with either StrepIII-HA-tagged wild-type (WT) PTPRA or CS mutants (C433S and C723S) along with V5-tagged RET expression vectors. The RET co-immunoprecipitates with all the PTPRA constructs. The immunoprecipitated (IP) proteins, as well as cell lysates, were immunoblotted with anti-V5 and anti-HA antibodies to detect RET and PTPRA proteins, respectively. The amount of immunoprecipitated tyrosine-phosphorylated RET was detected with a general anti-phosphotyrosine (pTyr) antibody. Tubulin is used as a loading control. See also Figure S3.

(E) PTPRA C433S mutant shows a significant decrease in RET activity in the Ras-MAPK luciferase-reporter assays, whereas C723S did not. The effect of CS mutation is measured in the absence (blue bars) and presence (orange bars) of GDNF-GFRα1 ligand co-complex (100–500 ng/mL; 24 h). The bar graph is representative of two independent experiments, where all bars indicate average ratios (n = 5 replicates) of Firefly to Renilla luciferase counts (relative luciferase unit, RLU) and the error bars designate one standard deviation. The statistical significance is obtained by a two-tailed Student's t test (***$p < 0.0001$).

(StrepIII-HA-tagged) together with RET (RET9; V5-tagged) (Figures 4B and S3A). As presented in Figure 4B, the RET co-precipitated with wild-type PTPRA as well as both DD mutants, which indicated that RET interacts with this phosphatase and might represent its physiological target. Noticeably, RET was predominantly recognized as a 150-kDa band (endoplasmic reticulum [ER] glycosylated species) in HEK293-MSR cells, which was explained previously by inefficient delivery of RET9 (1,072 amino acids) isoform from ER and Golgi to plasma membrane relative to another isoform RET51 (1,114 amino acids) in these cells (Iwamoto et al., 1993; Richardson et al., 2012; Takahashi et al., 1991).

Next, we examined the effect of PTPRA DD mutants (ΔD1 and ΔD2) in the RET-Ras-MAPK reporter assay. In this assay, the ΔD2 PTPRA mutant showed activity equivalent to the wild-type phosphatase post GDNF-GFRα1 stimulation, whereas the ΔD1 mutant failed to suppress the RET activity (Figure 4C). This demonstrates that the D1 domain is the main contributor toward RET inhibition, as well as highlights that the PTPRA membrane-proximal D1 domain contains most of the phosphatase catalytic activity toward RET.

To further understand the molecular details of PTPRA-RET interaction, we utilized PTPRA substrate-trapping (or phosphatase-dead) CS mutants (catalytic cysteine-to-serine): C433S (in D1 domain) and C723S (in D2 domain) (Figures 4A and S3A) (Den Hertog et al., 1994). The co-immunoprecipitation from HEK293-MSR cells, co-transfected with either wild-type or CS mutants of PTPRA (StrepIII-HA-tagged) and RET (V5-tagged), shows that both CS mutants could bind to (de)phosphorylated RET with no significant difference with wild-type PTPRA (Figure 4D). Also, the PTPRA interaction is greatly reduced with kinase-dead RET (K758R) mutants, suggesting that autophosphorylation of RET mediates this interaction (Figure S3B). However, in the luciferase assays, only C433S mutant leads to a greater (~2.7-fold; $p = 7.33 \times 10^{-7}$) dampening of reporter signal in contrast to C723S, indicating that C433S acts as a true substrate-tapping mutant and D1 domain catalytic activity is indeed required for PTPRA function (Figure 4E).

Taken together, although the D2 domain appeared to be non-essential for the RET-Ras-MAPK repression, it could be required for other possible PTPRA-substrate interactions or might play, if any, regulatory role.

PTPRA Instigates Direct Dephosphorylation of RET and Downstream RET Substrates

Furthermore, we explored the direct consequences of PTPRA phosphatase on tyrosine phosphorylation of RET kinase. Through *in vitro* phosphatase assay, where recombinant RET protein was incubated with either active PTPRA or recombinant GFP (control), we observed a significant decrease in RET tyrosine phosphorylation using general anti-phosphotyrosine (pTyr) antibody (Figure 5A). Moreover, LC-MS/MS-based phosphopeptide quantification (MaxQuant) of these samples showed the PTPRA-regulated dynamics of specific RET pTyr-sites (RET + GFP versus RET + PTPRA) (Figure 5A). Several conventional (known) RET pTyr-sites spanning juxtamembrane region, catalytic domain, and C-terminal tail such as Y752, Y826, Y981, and Y1015

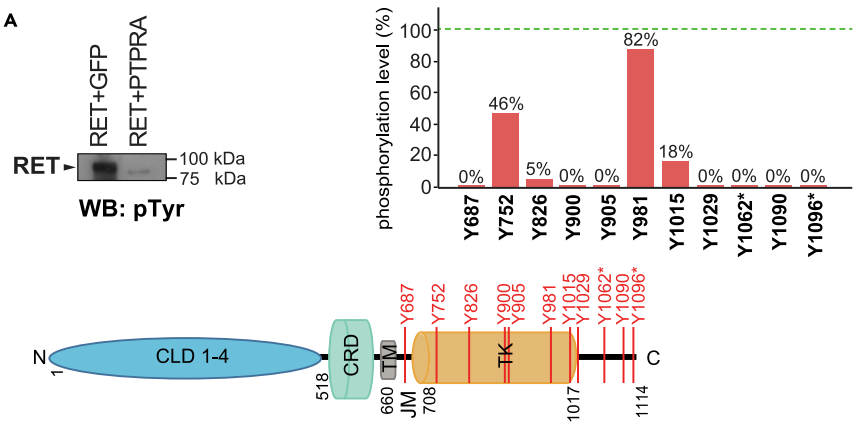
A
RET+GFP
RET+PTPRA
RET
100 kDa
75 kDa
WB: pTyr
phosphorylation level (%)
0%
46%
5%
0%
0%
82%
18%
0%
0%
0%
0%
Y687
Y752
Y826
Y900
Y905
Y981
Y1015
Y1029
Y1062*
Y1090
Y1096*
N
CLD 1-4
CRD
TM
JM
TK
C
1
518
660
708
1017
1114

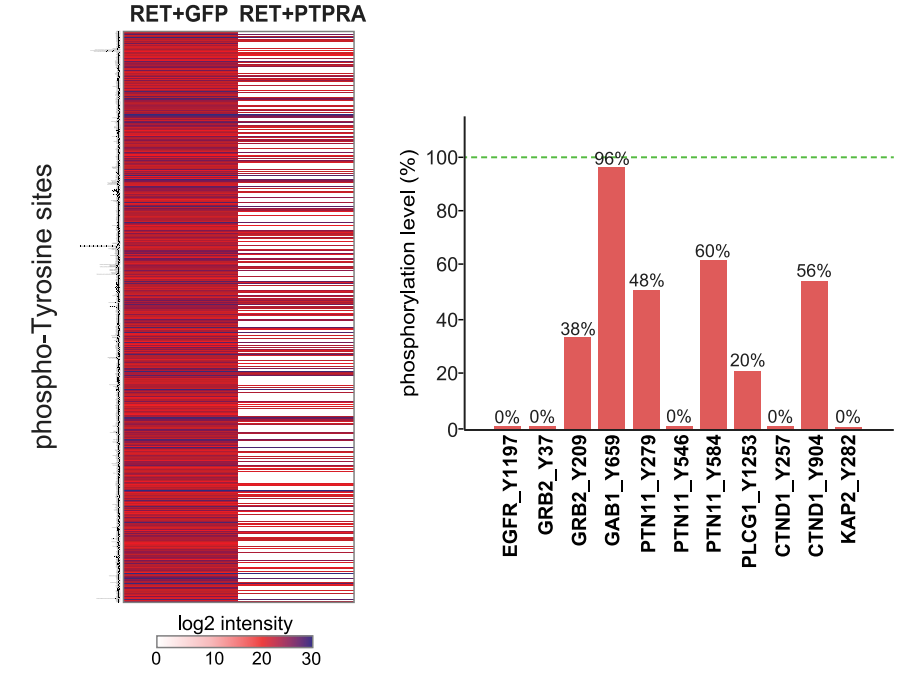
B
RET+GFP
RET+PTPRA
phospho-Tyrosine sites
log2 intensity
0
10
20
30
phosphorylation level (%)
0%
0%
38%
96%
48%
0%
60%
20%
0%
56%
0%
EGFR_Y1197
GRB2_Y37
GRB2_Y209
GAB1_Y659
PTN11_Y279
PTN11_Y546
PTN11_Y584
PLCG1_Y1253
CTND1_Y257
CTND1_Y904
KAP2_Y282

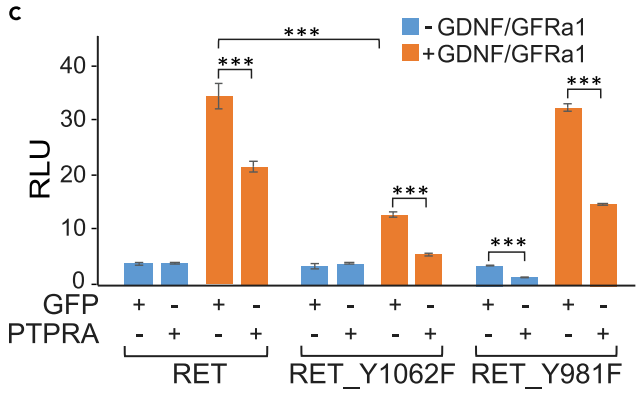
C
-GDNF/GFRa1
+GDNF/GFRa1
RLU
***
GFP
PTPRA
RET
RET_Y1062F
RET_Y981F

Figure 5. PTPRA Dephosphorylates RET and Regulates RET Kinase Activity

(A) The *in vitro* dephosphorylation of recombinant RET by recombinant PTPRA (active) or GFP (control) is checked with immunoblotting using an anti-pTyr antibody, where overall tyrosine phosphorylation of RET was significantly lowered in the presence of PTPRA. Also, the site-specific tyrosine phosphorylation changes of recombinant RET are detected with LC-MS/MS analysis, where several known phosphotyrosine (Y) sites (vertical red bars) on RET are effectively dephosphorylated by the PTPRA. The bar graph illustrates the percentage phosphorylation level of detected pTyr-sites in RET + PTPRA sample compared with control (RET + GFP), where the phosphorylation in control sample (i.e., maximum) is set to 100% (green dotted line). pTyr sites directly involved in RET-Ras-MAPK activation are marked with an asterisk (*). CLD1-4, cadherin-like domains 1–4; CRD, cysteine-rich domain; TM, transmembrane region; JM, juxtamembrane region; and TK, tyrosine kinase domain.

(B) The MS-based *in vitro* RET dephosphorylation assay shows the clear global inhibition of RET-mediated phosphorylation of pTyr sites on the HEK cell lysate proteins by PTPRA phosphatase. Phosphosites with localization probability score $\geq$0.75 are shown and log2 of the phosphopeptide intensities are depicted in the heat-map (scale bar, 0–30). Few known RET substrates also show a clear decrease in their indicated pTyr sites (Y) (% phosphorylation level; RET + PTPRA versus RET + GFP) in the presence of active PTPRA, shown as a bar graph. The phosphorylation in RET + GFP control sample (i.e., maximum) is set to 100% (green dotted line). See also Figure S4 and Table S2.

(C) Both Y1062 and Y981 are required for the RET activity on the Ras-MAPK pathway as displayed by the reporter assay activity. The Y1062 seems to be critical for RET activity, but both sites are regulated by the PTPRA as shown by using tyrosine (Y) to non-phosphorylatable phenylalanine (F) mutants:Y1062F and Y981F. The effect of PTPRA is measured in the absence (blue bars) and presence (orange bars) of GDNF-GFRα1 co-complex (100–500 ng/mL; 24 h). The data represent average ratios (n = 5 replicates) of the relative luciferase unit (RLU), and the error bars indicate one standard deviation. The statistical significance is obtained by a two-tailed Student's t test (***p < 0.0001).

underwent notable phosphorylation changes (54%, 95%, 17%, and 81% dephosphorylation, respectively), whereas Y687, Y900, Y905, Y1029, Y1062, Y1090, and Y1096 were completely dephosphorylated by PTPRA (Figure 5A). Interestingly, two of these phosphosites, Y1062 and Y1096, are shown to be critical for RET-Ras-MAPK activation (marked with an asterisk in Figure 5A) (Coulpier et al., 2002; Kawamoto et al., 2004). These results indicated that RET is a direct dephosphorylation target of PTPRA phosphatase and implied a potential enzyme-substrate relationship.

Then, we utilized a modified *in vitro* dephosphorylation assay coupled to mass spectrometry for obtaining the effects of PTPRA on cellular substrates of RET (Figures 5B and S4). Briefly, endogenous kinase deactivated (FSBA) cell lysate was incubated with recombinant RET and heavy ATP (ATP-$^{18}O_4$) in the presence or absence of recombinant PTPRA (Figure S4). The Ti^{4+}-IMAC enriched phosphopeptides were then analyzed using LC-MS/MS, revealing that the global tyrosine phosphorylation-profile of various candidate RET substrates was diminished by the PTPRA phosphatase activity (Figure 5B and Table S2). To our interest, several pTyr-sites on previously known RET substrates, also found in our PTPRA-RET interactome as part of the Ras-MAPK module, were clearly afflicted. For example, the phosphorylation status of Y209, Y279, Y548, Y1253, and Y904 sites in GRB2, PTN1, PLCG1, and CTND1, respectively, was greatly reduced (Figure 5B and Table S2). Moreover, phosphotyrosine sites in EGFR (Y1197), CTND1 (Y257), PTN1 (Y546), KAP2 (Y282), as well as GRB2 (Y37) proteins were completely lost in the presence of PTPRA (Table S2).

Among the above detected PTPRA-induced broad and site-specific RET phosphoproteomic changes, the autophosphorylation of Y1062 and Y981 has been shown in discrete oncogenic RET forms and is critical for GDNF-GFRα1-mediated neuronal signaling where Y1062 is vital for commencing Ras-MAPK as well as PI3K-AKT pathways and Y981 for Src activation (Asai et al., 1996; Coulpier et al., 2002; Encinas et al., 2004; Kawamoto et al., 2004). Therefore, we then mutated these sites to generate tyrosine (Y)-to-phenylalanine (F) mutants (Y1062F and Y981F) of RET and used them with PTPRA to analyze RET-Ras-MAPK signaling in a ligand-dependent manner. In the luciferase-reporter assay, the Y1062F mutant displayed much lower RET activity than the Y981F mutant in response to GDNF-GFRα1, suggesting that Y1062 is imperative for Ras-MAPK activation and directly contributes to RET regulation (Figure 5C). Surprisingly, with both RET-YF mutants PTPRA still prevented (up to 2-fold) the ligand-activated pathway response, which pointed toward other subsidiary RET pTyr sites that are likely to be affected by PTPRA and supported the phosphosite results obtained via MS-analysis.

PTPRA Restrains Oncogenic Potential of the RET Mutant MEN2A but Not MEN2B

We continued to broaden the participation of PTPRA phosphatase in controlling RET by studying its tumorigenic missense mutants, MEN2A and MEN2B, responsible for multiple endocrine neoplasms (MEN) of the thyroid and adrenal glands (Figure 6A). Reportedly, the MEN2A mutation (C634W) triggers RET by inducing

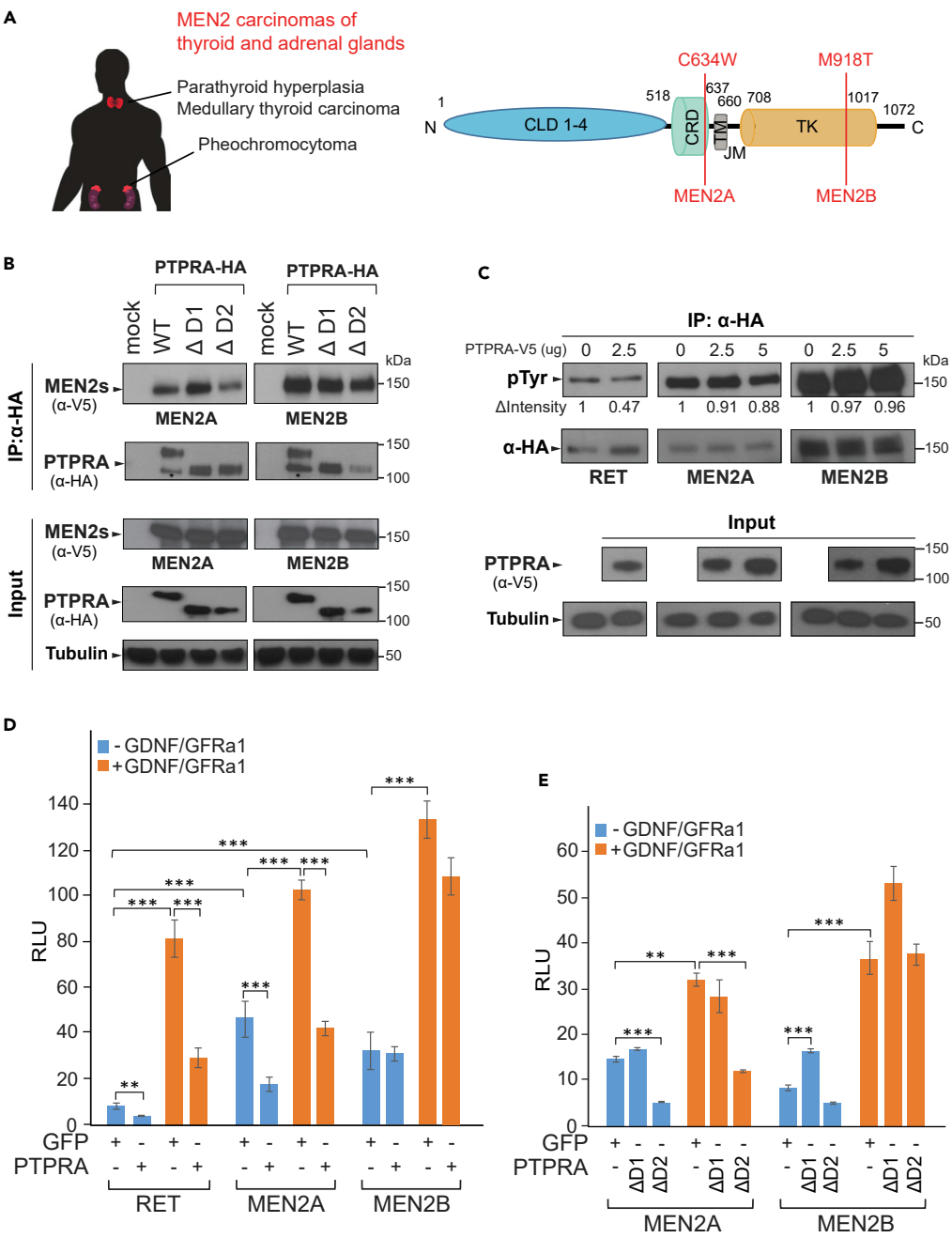

Figure 6. RET-MEN2A and -MEN2B Cancer Mutations and their Regulation by PTPRA

(A) RET-linked human multiple endocrine neoplasia (MEN) type 2 carcinomas, affecting the thyroid and adrenal glands. The corresponding MEN2 tumorigenic mutations (vertical red bars), MEN2A (C634W) and MEN2B (M918T), are in the RET CRD and TK domains, respectively. CLD1-4, cadherin-like domains 1–4; CRD, cysteine-rich domain; TM, transmembrane region; JM, juxtamembrane region; and TK, tyrosine kinase domain.

(B) PTPRA co-immunoprecipitates with both RET-MEN2A and -MEN2B mutants. V5-tagged RET-MEN2A or -MEN2B and either StrepIII-HA-tagged wild-type (WT) or phosphatase domain-deleted (DD: ΔD1 and ΔD2) mutants of PTPRA were expressed in HEK293-MSR cells. The immunoprecipitated (IP) proteins, as well as cell lysates, were immunoblotted with anti-V5 and anti-HA antibodies to detect RET-MEN2s and PTPRA proteins, respectively. Tubulin is used as a loading control (* unspecific band).

(C) *In vivo* tyrosine phosphorylation of RET and MEN2A, but not of MEN2B, successively decreases with the increasing amounts of PTPRA (0, 2.5, and 5 μg) construct. The RET and MEN2 (A and B) proteins were precipitated from cell lysates with anti-HA beads and immunoblotted with general anti-phosphotyrosine (pTyr) antibody. Equal gel loading is verified

Figure 6. *Continued*

by re-probing with anti-HA antibody, and relative intensity of pTyr level is analyzed by ImageJ software. PTPRA expression in cell lysate is determined by the anti-V5 antibody. Tubulin is used as a loading control.

(D) PTPRA efficiently inhibits the wild-type RET and MEN2A, whereas the MEN2B is less sensitive to the inhibition in the Ras-MAPK reporter assay, shown in the absence (blue bars) and presence (orange bars) of GDNF-GFRα1 ligands (100–500 ng/mL; 24 h). The bar graph is representative of two independent experiments, where all bars indicate average ratios (n = 5 replicates) of Firefly to Renilla luciferase counts (relative luciferase unit, RLU) and the error bars designate one standard deviation. The statistical significance is obtained by a two-tailed Student's t test (***$p < 0.0001$ and **$p < 0.001$). See also Table S3.

(E) Similarly to the wild-type RET, the ΔD2 mutant inhibits MEN2A but not MEN2B in the absence (blue bars) and presence (orange bars) of GDNF-GFRα1 ligands. Interestingly, the ΔD1 mutant slightly increases the MEN2B activity in our reporter assay. The bar graph is representative of two independent experiments, where all bars indicate average ratios (n = 5 replicates) of Firefly to Renilla luciferase counts (relative luciferase unit, RLU) and the error bars designate one standard deviation. The statistical significance is obtained by a two-tailed Student's t test (***$p < 0.0001$ and **$p < 0.001$).

ligand-independent homodimerization through abnormal intermolecular disulfide linkage, whereas the MEN2B mutation (M918T) stimulates the activity of RET monomer (Figure 6A) (Iwashita et al., 1996). This unusual intrinsic RET activation is liable for its high transforming ability and onset of atypical neurocristopathies (familial medullary thyroid carcinoma, papillary thyroid carcinoma, and pheochromocytomas). Therefore, we pursued to evaluate whether PTPRA can remodel the molecular and functional properties of these cancer-associated RET proteins. The co-immunoprecipitation of both MEN2A and MEN2B with wild-type PTPRA as well as its DD mutants established that, similar to wild-type RET, these RET mutants bind efficiently to PTPRA and might also serve as dephosphorylation targets of PTPRA in human cancers (Figures 4B and 6B). Therefore, when the general *in vivo* tyrosine phosphorylation level of these oncogenic RET forms was measured under varying levels of PTPRA (2.5 and 5 μg plasmid) in HEK293-MSR cells, we noted that phosphorylation of RET and MEN2A, but not of MEN2B, gradually decreased as the amount of PTPRA increased (Figure 6C).

We then conducted reporter assays with these oncogenic RET variants (MEN2s) in the presence of PTPRA and its DD mutants to check their individual effects on Ras-MAPK signaling. As expected, the baseline MEN2s-MAPK reporter activity was higher than the RET-MAPK activity, owing to the continuous signaling flux by the homodimeric MEN2A and monomeric MEN2B proteins (Figure 6D). Compared with luciferase intensity of wild-type RET alone, the MEN2A showed more pronounced (~5.5-fold; $p = 5.92 \times 10^{-7}$) basal activity than MEN2B (~3.8-fold; $p = 0.0001$) (Figure 6D). Additionally, the expression of PTPRA significantly attenuated MEN2A basal activation (~2.6-fold; $p = 6.7 \times 10^{-6}$), whereas that of MEN2B remained unchanged (Figure 6D). Surprisingly, GDNF-GFRα1 treatment still caused hyper-activation of both MEN2A and MEN2B reporter signals (~2.3- and ~4.5-fold, respectively) (Figures 6D and 6E). This could be due to the existence of hybrid receptor species between wild-type RET and MEN2 mutants, causing the additive response to ligand activation. However, this needs to be clarified in the future. Nevertheless, the data under these ligand-activated conditions also correlate well with the basal pathway activation results, where MEN2A-MAPK pathway activity (but not MEN2B) was again significantly inhibited (~2.5-fold; $p = 2.39 \times 10^{-9}$) by PTPRA co-expression (Figure 6D). Furthermore, in corresponding assays of PTPRA DD mutants (ΔD1 and ΔD2) with MEN2A and MEN2B proteins, PTPRA ΔD2 mutant inhibited the MEN2A-MAPK activity significantly (~3.2-fold) (Figure 6E). Unexpectedly, ΔD1 mutant enhanced (~1.9-fold; $p = 5.14 \times 10^{-5}$) the basal MEN2B-MAPK activity, for which the exact reason is not known and requires further investigation.

Because MEN2B-MAPK signaling was not modified by PTPRA (or DD mutants), irrespective of the ligand addition, we reasoned that PTPRA prefers dimeric configuration of MEN2A over the monomeric state of MEN2B to exert substrate inhibition. Alternatively, we evaluated the *in vivo* MS phosphorylation difference between RET and MEN2 mutants in the presence of GDNF-GFRα1 ligands as well as monitored whether their pTyr sites are impaired by PTPRA. The peptides and phosphosites (without phosphoenrichment) identified in these samples are listed in Table S3. Relatively more pTyr sites were detected for MEN2A (eight sites) than for RET and MEN2B (three sites each), which was in line with the RET and MEN2s phosphorylation levels in our reporter assays (Figures 6D and 6E and Table S3). Moreover, MEN2A and MEN2B harbored discrete phosphopeptide profiles. Under this setup, PTPRA reduced the phosphopeptide intensities of RET and MEN2A pTyr sites to a larger extent than MEN2B sites, demonstrating the basis of MEN2B resistance to PTPRA action (Table S3).

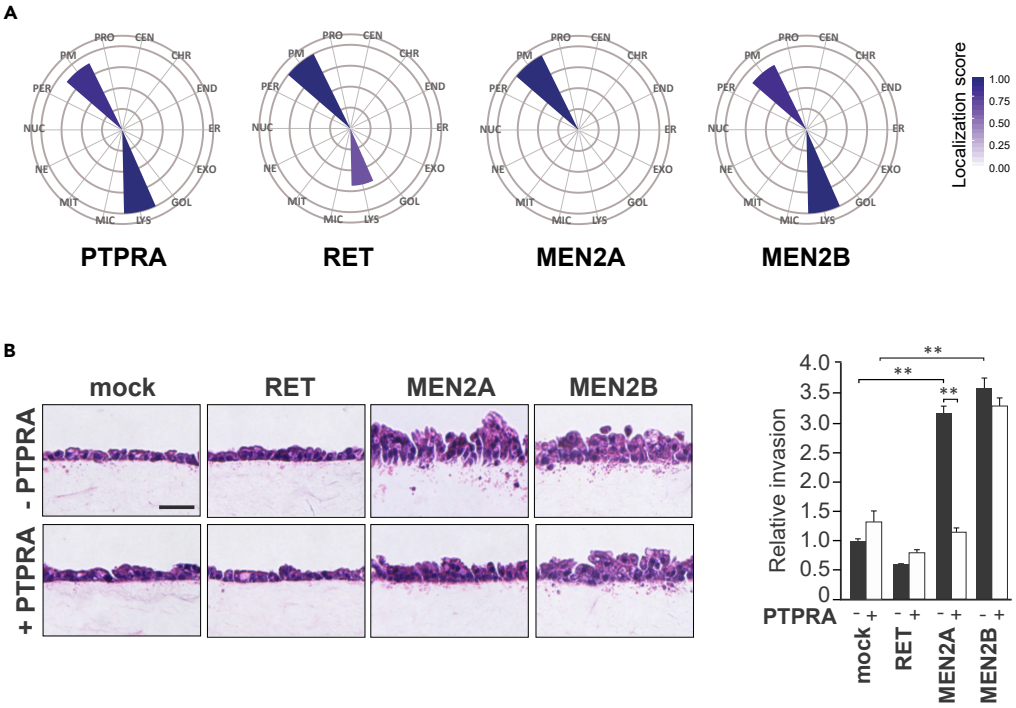

Figure 7. PTPRA Inhibits the RET Mutant MEN2A-induced Invasion

(A) Mass spectrometry (MS)-microscopy analysis of RET, MEN2A-B, and PTPRA subcellular localization. The cellular localization context of RET, MEN2A-B, and PTPRA interactors identified through the BioID method. The circular polar plot is divided into 14 different cellular compartments: centrosome (CEN), chromatin (CHR), endosome (END), endoplasmic reticulum (ER), exosome (EXO), Golgi (GOL), lysosome (LYS), microtubule (MIC), mitochondria (MIT), nuclear envelope (NE), nucleolus (NUC), peroxisome (PER), plasma membrane (PM), and proteasome (PRO). The color gradient indicates the localization scores (scale bar, 0–1) calculated by the MS-microscopy tool. See also Figure S5.

(B) PTPRA inhibits the MEN2A-induced cell invasion. The light micrographs of the hematoxylin and eosin-stained MDCK cells co-expressing MEN2A or MEN2B along with control vector (mock) or PTPRA plasmids show reduced cell invasion

Figure 7. *Continued*

when PTPRA is present (scale bar, 20 μm). The bar graph shows the quantitated relative invasion, where the invasion of mock cells is set to one. The error bars indicate mean ± SEM (standard error of the mean, n = 6) and **$p < 0.001$ defines the significance, calculated from a two-tailed Student's t test.

(C) Model for signaling regulation mediated by RET and PTPRA interaction. By binding to dimeric RET and oncogenic mutant MEN2A (C634W), PTPRA limits the RET and MEN2A phosphorylation along with downstream Ras-MAPK activation. However, monomeric MEN2B (M918T) RET mutant refrains from PTPRA inhibition. As a consequence, by hindering abnormal cancer traits, such as cell invasion, through RET regulation, this model demarks the plausible anti-cancer role of PTPRA in medullary thyroid cancer, pheochromocytomas, and parathyroid adenomas. CAD, cadherin-like domain; CYS, cysteine-rich domain; ECD, extracellular domain; JM, juxtamembrane region; P, phosphate group; PTPase, protein tyrosine phosphatase domain; TK, tyrosine kinase domain; and TM, transmembrane region.

Also of interest is the likelihood that the MEN2B localization would also differ from the wild-type RET and MEN2A mutant. To assess these spatial prospects, the molecular context of PTPRA and RET variants was derived from the BioID data using mass spectrometry (MS)-microscopy approach, where they were predominantly enriched in the plasma membrane (Figure 7A and Table S1) (Liu et al., 2018). However, MEN2A exclusively displayed plasma membrane localization in a manner identical to the ligand-induced aggregation of receptors on the cell surface. Additionally, the co-localization was also inspected in HeLa cells with fluorescent microscopy, where PTPRA showed comparable colocalization signal with RET and MEN2A (Figure S5).

PTPRA Suppresses the MEN2A-Induced Invasion

Finally, to assess the possible role of PTPRA in limiting certain RET mutants' cancer-causing traits, we performed a three-dimensional (3D) collagen invasion assay using the MDCK cell model. These cells display characteristic epithelial basolateral polarity and directional phenotypic transition in response to their growth environment (Zak et al., 2000). In this model, wild-type RET-expressing cells were minimally invasive, whereas both MEN2A- and MEN2B-expressing cells showed enhanced baseline invasiveness (up to 5-fold) towards GDNF-GFRα1 ligands (used as chemoattractants), which indicated the severity of these cancer-associated mutations in tumor progression (Figure 7B). This robust phenotype was antagonized by the co-incorporation of PTPRA, where it significantly decreased (3-fold) the migration potential of MEN2A mutant (Figure 7B). By contrast, the MEN2B-expressing cells remained insensitive to PTPRA-mediated suppression of chemotaxis and invasion. Because invasion across extracellular matrix constraint is prevalent to cancer metastasis, these facets of PTPRA effects on cell invasion in our 3D collagen model uncovers PTPRA as an immediate regulator with a probable anti-cancer role in steering RET-Ras-MAPK signaling.

Concluding Remark

PTPRA is expressed widely in human neuronal cells (brain, thyroid, testis, and kidney) and their associated cancers (astrocytoma, mixed glioma, thyroid carcinoma, renal cell carcinoma, and nephroblastoma). Previously, PTPRA has been shown to regulate a few growth factor-dependent signaling by dephosphorylating only a minority of cytoplasmic- and receptor-tyrosine kinases (Src, Fyn, and EGFR). Hence, the other critical functional primary cellular targets of PTPRA have remained as yet unknown. Thus, we investigated the role of PTPRA in GDNF-activated RET-Ras-MAPK signaling and obtained extensive physical and functional interactions between PTPRA and RET complexes. For example, neurotrophic factor GDNF and different adaptors (GRB2, GAB1, and FRS2) collectively interacted with both PTPRA and RET. These along with other adaptor proteins (Src, SOS1-2, SHC1, and SHB) have been reported as components of neuronal RET-Ras-MAPK signaling, and their association with PTPRA in our study proposed its relevance in coordinating RET intracellular signaling (Besset et al., 2000; Katz et al., 2007). Moreover, we demonstrated that PTPRA significantly inhibits the GDNF-GFRα1-induced RET-Ras-MAPK pathway activity, indicating the negative regulation imposed by PTPRA. We also showed the decreased phosphorylation levels of downstream MAPKs ERK1 and ERK2, suggesting that RET is a primary target of PTPRA. Of note, by using PTPRA Y789F mutant we established the role of proximate adaptor protein GRB2 in the context of RET-mediated Ras-MAPK signaling. Surprisingly, the response of PTPRA on overall Ras-MAPK signaling in our study contradicted with that of Yao et al. (2017), where PTPRA was shown to positively influence the EGFR-driven Ras-MAPK signaling. Nevertheless, the reason, to some extent, might lie in the composition of RET and EGFR signaling complexes, as evinced by their unique interactomes (~10% overlap) obtained through proteomic analysis. Then, using phosphatase domain (PTPase) deletion (D1 and D2) and catalytically inactive CS point mutants, we not only established direct physical

interaction between PTPRA and RET but also mapped the functional domain required for its molecular activity. We further revealed that PTPRA influences the overall (*in vitro*) tyrosine phosphorylation profile of RET and its candidate cellular substrates such as GRB2, PLCG1, EGFR, and KAP2, which displayed either complete loss or a significant decrease in their tyrosine phosphorylation. Additionally, many tyrosine sites on RET itself (Y826, Y981, Y1015, Y1062, and Y1096) were inflicted by PTPRA, suggesting that RET is directly dephosphorylated by this phosphatase. Besides that, the MS-based phosphoproteomic results of *in vivo* RET dephosphorylation by PTPRA after ligand-activation confirmed that the functional outcome of RET is indeed reshaped by PTPRA and explained the prevalent Ras-MAPK activation inhibition. We also inspected the plausible role of PTPRA in inhibiting the cancer-causing attributes of RET thyroid carcinoma mutants MEN2A and MEN2B. The results showed that PTPRA inhibited the MEN2A-Ras-MAPK activation and effectively dephosphorylated MEN2A, whereas MEN2B resisted this. Notably, MEN2B (M918T) mutation is located in the RET catalytic domain, which might disrupt its conformation and alter *in vivo* substrate specificity. This could explain the unresponsiveness of MEN2B toward PTPRA inhibition, despite its physical interaction with PTPRA. However, with MS we identified the distinct phosphorylation profiles (*in vivo*) of MEN2s post GDNF-GFRα1 activation, which revealed the grounds for their differential activity and response to PTPRA action. Finally, we disclosed the biological consequences of MEN2A and MEN2B dephosphorylation by PTPRA on the regulation of cell invasion, whereby it drastically reduced the MDCK cell invasion induced by MEN2A oncogene in 3D collagen, a matrix that typifies the primary and metastatic tumor tissue microenvironments. Because MEN2B is clinically more aggressive than other MEN2 subtypes, the *inertness* of this RET mutant receptor to overall PTPRA adjustment successfully justifies for its high oncogenic activity in thyroid carcinomas.

To conclude, our study provides compelling evidence that PTPRA regulates GDNF-dependent RET-Ras-MAPK growth signaling by inhibiting the molecular activities of both RET and MEN2A via dephosphorylation (Figure 7C), thus making PTPRA indispensable for balancing RET activity and function in both health and disease.

Limitations of the Study

We have demonstrated many common interacting proteins, statistically obtained in a data-dependent manner, for both RET and PTPRA using AP-MS and BioID proteomic analysis. A subset of interacting proteins included several cell-surface receptors and docking proteins, as well as proteins involved in neuronal development, polarization, axon guidance, pathfinding, and pattern/axis formation. It may be important to validate these interactors for GDNF-associated RET-Ras-MAPK signaling. Besides, we have shown that PTPRA directly dephosphorylates RET and modulates the GDNF-activated RET-Ras-MAPK pathway; however, one may check the reaction (dephosphorylation) kinetics.

METHODS

All methods can be found in the accompanying Transparent Methods supplemental file.

DATA AND CODE AVAILABILITY

All reagents are available within Transparent Methods section of the accompanying Supplemental Information text file. The requests for resources and reagents may be directed to and will be fulfilled by the Lead Contact, Markku Varjosalo (markku.varjosalo@helsinki.fi). The plasmids are made available via Addgene.org.

SUPPLEMENTAL INFORMATION

Supplemental Information can be found online at https://doi.org/10.1016/j.isci.2020.100871.

ACKNOWLEDGMENTS

We acknowledge Sini Miettinen and Jenni Montonen for excellent technical assistance. This work was supported by grants from the Academy of Finland (Nos. 288475 and 294173), Sigrid Juselius Foundation (to M.V., K.L., and M.S.), Finnish Cancer Foundation (to M.V. and K.L.), University of Helsinki three-year research grant, Biocentrum Helsinki, Biocentrum Finland, and Instrumentarium Research Foundation.

AUTHOR CONTRIBUTIONS

M.V. and L.Y. conceived and designed the study. L.Y. performed majority of the experiments, analyzed, and organized the results. A.K.M. and Y.S. participated in PTPRA intervention experiments. T.Ö., E.P., K.L., and X.L. performed and interpreted the *in vitro* dephosphorylation assay, cell invasion assay, and fluorescent microscopy, respectively. L.Y. and M.V. wrote the manuscript with the input from T.Ö., K.L., and M.S.

DECLARATION OF INTERESTS

The authors declare no competing interest.

Received: August 3, 2019
Revised: January 15, 2020
Accepted: January 26, 2020
Published: February 21, 2020

REFERENCES

Airaksinen, M.S., and Saarma, M. (2002). The GDNF family: signalling, biological functions and therapeutic value. Nat. Rev. Neurosci. *3*, 383–394.

Alberti, L., Borrello, M.G., Ghizzoni, S., Torriti, F., Rizzetti, M.G., and Pierotti, M.A. (1998). Grb2 binding to the different isoforms of Ret tyrosine kinase. Oncogene *17*, 1079–1087.

Amoresano, A., Incoronato, M., Monti, G., Pucci, P., De Franciscis, V., and Cerchia, L. (2005). Direct interactions among Ret, GDNF and GFRalpha1 molecules reveal new insights into the assembly of a functional three-protein complex. Cell Signal. *17*, 717–727.

Arighi, E., Borrello, M.G., and Sariola, H. (2005). RET tyrosine kinase signaling in development and cancer. Cytokine Growth Factor Rev. *16*, 441–467.

Asai, N., Murakami, H., Iwashita, T., and Takahashi, M. (1996). A mutation at tyrosine 1062 in MEN2A-Ret and MEN2B-Ret impairs their transforming activity and association with Shc adaptor proteins. J. Biol. Chem. *271*, 17644–17649.

Besset, V., Scott, R.P., and Ibanez, C.F. (2000). Signaling complexes and protein-protein interactions involved in the activation of the Ras and phosphatidylinositol 3-kinase pathways by the c-Ret receptor tyrosine kinase. J. Biol. Chem. *275*, 39159–39166.

Bodrikov, V., Leshchyns'ka, I., Sytnyk, V., Overvoorde, J., Den Hertog, J., and Schachner, M. (2005). RPTPalpha is essential for NCAM-mediated p59fyn activation and neurite elongation. J. Cell Biol. *168*, 127–139.

Chen, S.C., Khanna, R.S., Bessette, D.C., Samayawardhena, L.A., and Pallen, C.J. (2009). Protein tyrosine phosphatase-alpha complexes with the IGF-I receptor and undergoes IGF-I-stimulated tyrosine phosphorylation that mediates cell migration. Am. J. Physiol. Cell Physiol. *297*, C133–C139.

Chen, Y.M., Wang, Q.J., Hu, H.S., Yu, P.C., Zhu, J., Drewes, G., Piwnica-Worms, H., and Luo, Z.G. (2006). Microtubule affinity-regulating kinase 2 functions downstream of the PAR-3/PAR-6/atypical PKC complex in regulating hippocampal neuronal polarity. Proc. Natl. Acad. Sci. U S A *103*, 8534–8539.

Costantini, F., and Shakya, R. (2006). GDNF/Ret signaling and the development of the kidney. Bioessays *28*, 117–127.

Coulpier, M., Anders, J., and Ibanez, C.F. (2002). Coordinated activation of autophosphorylation sites in the RET receptor tyrosine kinase: importance of tyrosine 1062 for GDNF mediated neuronal differentiation and survival. J. Biol. Chem. *277*, 1991–1999.

Daum, G., Regenass, S., Sap, J., Schlessinger, J., and Fischer, E.H. (1994). Multiple forms of the human tyrosine phosphatase RPTP alpha. Isozymes and differences in glycosylation. J. Biol. Chem. *269*, 10524–10528.

Den Hertog, J., Tracy, S., and Hunter, T. (1994). Phosphorylation of receptor protein-tyrosine phosphatase alpha on Tyr789, a binding site for the SH3-SH2-SH3 adaptor protein GRB-2 in vivo. EMBO J. *13*, 3020–3032.

Denardo, B.D., Holloway, M.P., Ji, Q., Nguyen, K.T., Cheng, Y., Valentine, M.B., Salomon, A., and Altura, R.A. (2013). Quantitative phosphoproteomic analysis identifies activation of the RET and IGF-1R/IR signaling pathways in neuroblastoma. PLoS One *8*, e82513.

Denhertog, J., and Hunter, T. (1996). Tight association of GRB2 with receptor protein-tyrosine phosphatase alpha is mediated by the SH2 and c-terminal SH3 domains. EMBO J. *15*, 3016–3027.

Drinkut, A., Tillack, K., Meka, D.P., Schulz, J.B., Kugler, S., and Kramer, E.R. (2016). Ret is essential to mediate GDNF's neuroprotective and neuroregenerative effect in a Parkinson disease mouse model. Cell Death Dis. *7*, e2359.

Eketjall, S., Fainzilber, M., Murray-Rust, J., and Ibanez, C.F. (1999). Distinct structural elements in GDNF mediate binding to GFRalpha1 and activation of the GFRalpha1-c-Ret receptor complex. EMBO J. *18*, 5901–5910.

Encinas, M., Crowder, R.J., Milbrandt, J., and Johnson, E.M., Jr. (2004). Tyrosine 981, a novel ret autophosphorylation site, binds c-Src to mediate neuronal survival. J. Biol. Chem. *279*, 18262–18269.

Eng, C., and Mulligan, L.M. (1997). Mutations of the RET proto-oncogene in the multiple endocrine neoplasia type 2 syndromes, related sporadic tumours, and Hirschsprung disease. Hum. Mutat. *9*, 97–109.

Geiger, T., Wehner, A., Schaab, C., Cox, J., and Mann, M. (2012). Comparative proteomic analysis of eleven common cell lines reveals ubiquitous but varying expression of most proteins. Mol. Cell Proteomics *11*, M111 014050.

Goodman, K.M., Kjaer, S., Beuron, F., Knowles, P.P., Nawrotek, A., Burns, E.M., Purkiss, A.G., George, R., Santoro, M., Morris, E.P., et al. (2014). RET recognition of GDNF-GFRalpha1 ligand by a composite binding site promotes membrane-proximal self-association. Cell Rep. *8*, 1894–1904.

Hennige, A.M., Lammers, R., Hoppner, W., Arlt, D., Strack, V., Teichmann, R., Machicao, F., Ullrich, A., Haring, H.U., and Kellerer, M. (2001). Inhibition of Ret oncogene activity by the protein tyrosine phosphatase SHP1. Endocrinology *142*, 4441–4447.

Huang, J., Yao, L., Xu, R., Wu, H., Wang, M., White, B.S., Shalloway, D., and Zheng, X. (2011). Activation of Src and transformation by an RPTPalpha splice mutant found in human tumours. EMBO J. *30*, 3200–3211.

Imbrici, P., Tucker, S.J., D'adamo, M.C., and Pessia, M. (2000). Role of receptor protein tyrosine phosphatase alpha (RPTPalpha) and tyrosine phosphorylation in the serotonergic inhibition of voltage-dependent potassium channels. Pflugers Arch. *441*, 257–262.

Imgrund, S., Hartmann, D., Farwanah, H., Eckhardt, M., Sandhoff, R., Degen, J., Gieselmann, V., Sandhoff, K., and Willecke, K. (2009). Adult ceramide synthase 2 (CERS2)-deficient mice exhibit myelin sheath defects, cerebellar degeneration, and hepatocarcinomas. J. Biol. Chem. *284*, 33549–33560.

Iwamoto, T., Taniguchi, M., Asai, N., Ohkusu, K., Nakashima, I., and Takahashi, M. (1993). cDNA cloning of mouse ret proto-oncogene and its sequence similarity to the cadherin superfamily. Oncogene *8*, 1087–1091.

Iwashita, T., Asai, N., Murakami, H., Matsuyama, M., and Takahashi, M. (1996). Identification of tyrosine residues that are essential for transforming activity of the ret proto-oncogene

with MEN2A or MEN2B mutation. Oncogene *12*, 481–487.

Kaplan, R., Morse, B., Huebner, K., Croce, C., Howk, R., Ravera, M., Ricca, G., Jaye, M., and Schlessinger, J. (1990). Cloning of three human tyrosine phosphatases reveals a multigene family of receptor-linked protein-tyrosine-phosphatases expressed in brain. Proc. Natl. Acad. Sci. U S A *87*, 7000–7004.

Kapp, K., Metzinger, E., Kellerer, M., Haring, H.U., and Lammers, R. (2003). The protein tyrosine phosphatase alpha modifies insulin secretion in INS-1E cells. Biochem. Biophys. Res. Commun. *311*, 361–364.

Katz, M., Amit, I., and Yarden, Y. (2007). Regulation of MAPKs by growth factors and receptor tyrosine kinases. Biochim. Biophys. Acta *1773*, 1161–1176.

Kawamoto, Y., Takeda, K., Okuno, Y., Yamakawa, Y., Ito, Y., Taguchi, R., Kato, M., Suzuki, H., Takahashi, M., and Nakashima, I. (2004). Identification of RET autophosphorylation sites by mass spectrometry. J. Biol. Chem. *279*, 14213–14224.

Larrivee, B., Freitas, C., Trombe, M., Lv, X., Delafarge, B., Yuan, L., Bouvree, K., Breant, C., Del Toro, R., Brechot, N., et al. (2007). Activation of the UNC5B receptor by Netrin-1 inhibits sprouting angiogenesis. Genes Dev. *21*, 2433–2447.

Li, L., Su, Y., Zhao, C., Zhao, H., Liu, G., Wang, J., and Xu, Q. (2006). The role of Ret receptor tyrosine kinase in dopaminergic neuron development. Neuroscience *142*, 391–400.

Liu, X., Salokas, K., Tamene, F., Jiu, Y., Weldatsadik, R.G., Ohman, T., and Varjosalo, M. (2018). An AP-MS- and BioID-compatible MAC-tag enables comprehensive mapping of protein interactions and subcellular localizations. Nat. Commun. *9*, 1188.

Melillo, R.M., Santoro, M., Ong, S.H., Billaud, M., Fusco, A., Hadari, Y.R., Schlessinger, J., and Lax, I. (2001). Docking protein FRS2 links the protein tyrosine kinase RET and its oncogenic forms with the mitogen-activated protein kinase signaling cascade. Mol. Cell Biol. *21*, 4177–4187.

Mosevitsky, M.I. (2005). Nerve ending "signal" proteins GAP-43, MARCKS, and BASP1. Int. Rev. Cytol. *245*, 245–325.

Mulligan, L.M. (2014). RET revisited: expanding the oncogenic portfolio. Nat. Rev. Cancer *14*, 173–186.

Norman, R.X., Ko, H.W., Huang, V., Eun, C.M., Abler, L.L., Zhang, Z., Sun, X., and Eggenschwiler, J.T. (2009). Tubby-like protein 3 (TULP3) regulates patterning in the mouse embryo through inhibition of Hedgehog signaling. Hum. Mol. Genet. *18*, 1740–1754.

Norris, K., Norris, F., Kono, D.H., Vestergaard, H., Pedersen, O., Theofilopoulos, A.N., and Moller, N.P. (1997). Expression of protein-tyrosine phosphatases in the major insulin target tissues. FEBS Lett. *415*, 243–248.

Ohiwa, M., Murakami, H., Iwashita, T., Asai, N., Iwata, Y., Imai, T., Funahashi, H., Takagi, H., and Takahashi, M. (1997). Characterization of Ret-Shc-Grb2 complex induced by GDNF, MEN 2A, and MEN 2B mutations. Biochem. Biophys. Res. Commun. *237*, 747–751.

Pachnis, V., Mankoo, B., and Costantini, F. (1993). Expression of the c-ret proto-oncogene during mouse embryogenesis. Development *119*, 1005–1017.

Perrinjaquet, M., Vilar, M., and Ibanez, C.F. (2010). Protein-tyrosine phosphatase SHP2 contributes to GDNF neurotrophic activity through direct binding to phospho-Tyr687 in the RET receptor tyrosine kinase. J. Biol. Chem. *285*, 31867–31875.

Petrone, A., Battaglia, F., Wang, C., Dusa, A., Su, J., Zagzag, D., Bianchi, R., Casaccia-Bonnefil, P., Arancio, O., and Sap, J. (2003). Receptor protein tyrosine phosphatase alpha is essential for hippocampal neuronal migration and long-term potentiation. EMBO J. *22*, 4121–4131.

Poliak, S., Morales, D., Croteau, L.P., Krawchuk, D., Palmesino, E., Morton, S., Cloutier, J.F., Charron, F., Dalva, M.B., Ackerman, S.L., et al. (2015). Synergistic integration of Netrin and ephrin axon guidance signals by spinal motor neurons. Elife *4*, https://doi.org/10.7554/eLife.10841.

Qiao, S., Iwashita, T., Furukawa, T., Yamamoto, M., Sobue, G., and Takahashi, M. (2001). Differential effects of leukocyte common antigen-related protein on biochemical and biological activities of RET-MEN2A and RET-MEN2B mutant proteins. J. Biol. Chem. *276*, 9460–9467.

Richardson, D.S., Rodrigues, D.M., Hyndman, B.D., Crupi, M.J., Nicolescu, A.C., and Mulligan, L.M. (2012). Alternative splicing results in RET isoforms with distinct trafficking properties. Mol. Biol. Cell *23*, 3838–3850.

Santoro, M., Melillo, R.M., Carlomagno, F., Vecchio, G., and Fusco, A. (2004). Minireview: ret: normal and abnormal functions. Endocrinology *145*, 5448–5451.

Schedl, A. (2007). Renal abnormalities and their developmental origin. Nat. Rev. Genet. *8*, 791–802.

Soba, P., Han, C., Zheng, Y., Perea, D., Miguel-Aliaga, I., Jan, L.Y., and Jan, Y.N. (2015). The Ret receptor regulates sensory neuron dendrite growth and integrin mediated adhesion. Elife *4*, https://doi.org/10.7554/eLife.05491.

Takahashi, M., Buma, Y., and Taniguchi, M. (1991). Identification of the ret proto-oncogene products in neuroblastoma and leukemia cells. Oncogene *6*, 297–301.

Telley, L., Cadilhac, C., Cioni, J.M., Saywell, V., Jahannault-Talignani, C., Huettl, R.E., Sarrailh-Faivre, C., Dayer, A., Huber, A.B., and Ango, F. (2016). Dual function of NRP1 in axon guidance and subcellular target recognition in cerebellum. Neuron *91*, 1276–1291.

Torban, E., Wang, H.J., Groulx, N., and Gros, P. (2004). Independent mutations in mouse Vangl2 that cause neural tube defects in looptail mice impair interaction with members of the Dishevelled family. J. Biol. Chem. *279*, 52703–52713.

Tremper-Wells, B., Resnick, R.J., Zheng, X., Holsinger, L.J., and Shalloway, D. (2010). Extracellular domain dependence of PTPalpha transforming activity. Genes Cells *15*, 711–724.

Truffi, M., Dubreuil, V., Liang, X., Vacaresse, N., Nigon, F., Han, S.P., Yap, A.S., Gomez, G.A., and Sap, J. (2014). RPTPalpha controls epithelial adherens junctions, linking E-cadherin engagement to c-Src-mediated phosphorylation of cortactin. J. Cell Sci. *127*, 2420–2432.

Wang, Y., and Pallen, C.J. (1991). The receptor-like protein tyrosine phosphatase HPTP alpha has two active catalytic domains with distinct substrate specificities. EMBO J. *10*, 3231–3237.

Wu, L., Buist, A., Den Hertog, J., and Zhang, Z.Y. (1997). Comparative kinetic analysis and substrate specificity of the tandem catalytic domains of the receptor-like protein-tyrosine phosphatase alpha. J. Biol. Chem. *272*, 6994–7002.

Xiao, Q., Rongfei, W., Lingqiang, Z., and Fuchu, H. (2015). The roles of signaling pathways in regulating kidney development. Yi Chuan *37*, 1–7.

Yadav, L., Tamene, F., Goos, H., Van Drogen, A., Katainen, R., Aebersold, R., Gstaiger, M., and Varjosalo, M. (2017). Systematic analysis of human protein phosphatase interactions and dynamics. Cell Syst. *4*, 430–444.e5.

Yao, Z., Darowski, K., St-Denis, N., Wong, V., Offensperger, F., Villedieu, A., Amin, S., Malty, R., Aoki, H., Guo, H., et al. (2017). A global analysis of the receptor tyrosine kinase-protein phosphatase interactome. Mol. Cell *65*, 347–360.

Zak, J., Schneider, S.W., Eue, I., Ludwig, T., and Oberleithner, H. (2000). High-resistance MDCK-C7 monolayers used for measuring invasive potency of tumour cells. Pflugers Arch. *440*, 179–183.

Zheng, X.M., Resnick, R.J., and Shalloway, D. (2000). A phosphotyrosine displacement mechanism for activation of Src by PTPalpha. EMBO J. *19*, 964–978.

Zheng, X.M., Resnick, R.J., and Shalloway, D. (2002). Mitotic activation of protein-tyrosine phosphatase alpha and regulation of its Src-mediated transforming activity by its sites of protein kinase C phosphorylation. J. Biol. Chem. *277*, 21922–21929.

iScience, Volume *23*

Supplemental Information

PTPRA Phosphatase Regulates GDNF-Dependent RET Signaling and Inhibits the RET Mutant MEN2A Oncogenic Potential

Leena Yadav, Elina Pietilä, Tiina Öhman, Xiaonan Liu, Arun K. Mahato, Yulia Sidorova, Kaisa Lehti, Mart Saarma, and Markku Varjosalo

Figure S1. PTPRA and RET interactome overlap with EGFR, ERBB2, and IGF1R kinases, related to Figure 1B

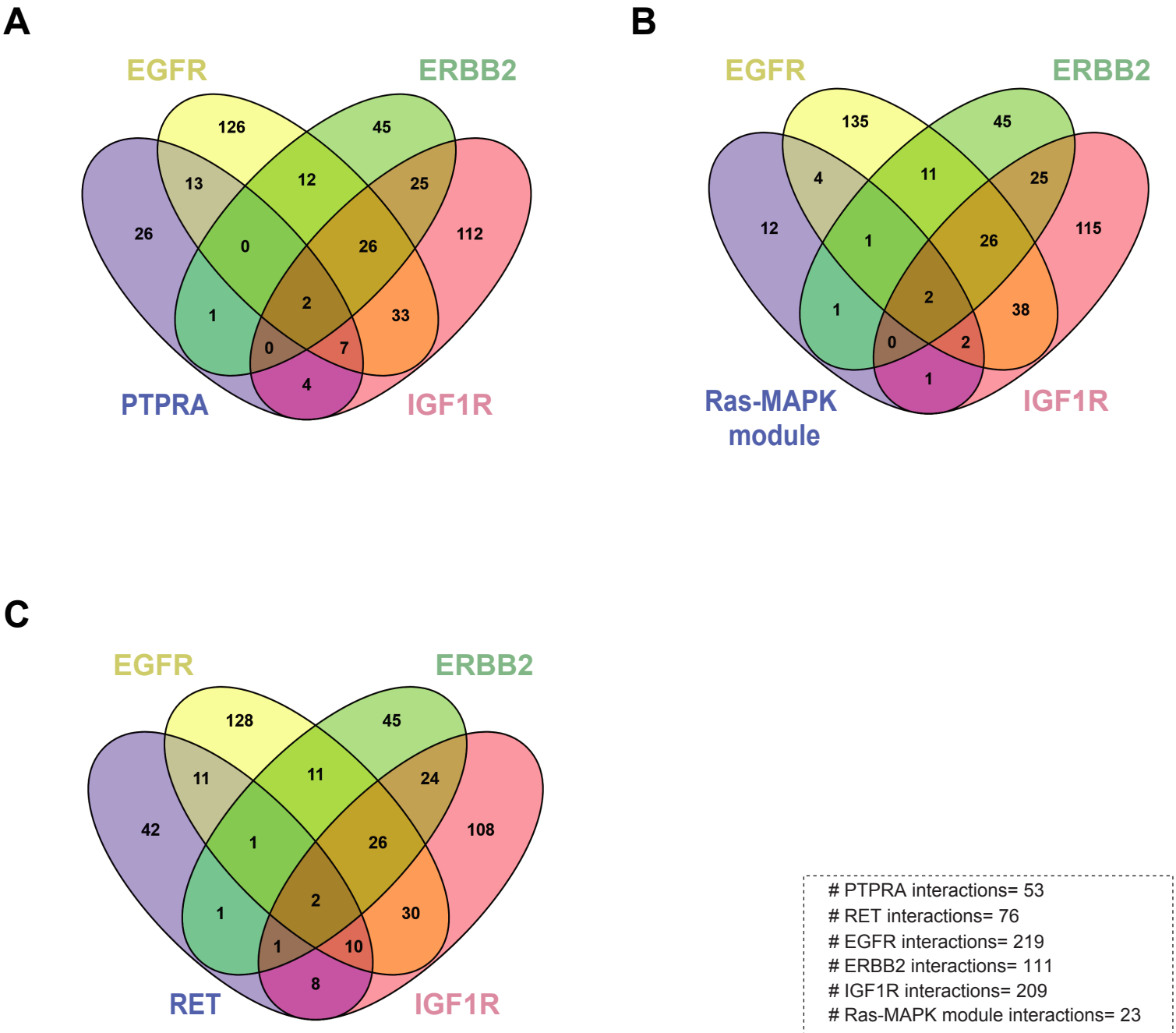

Figure S2. Tissue-specific gene expression pattern of PTPRA, related to Figure 1

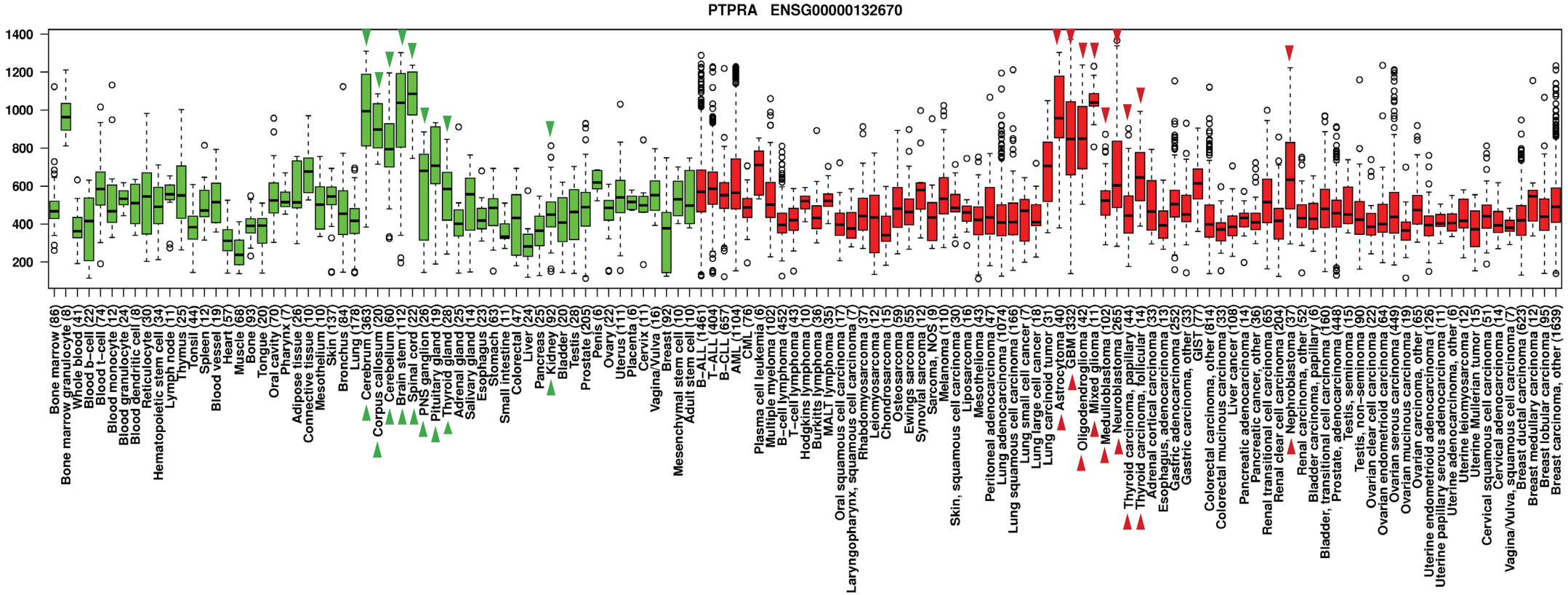

Figure S3. Expression of PTPRA mutants and interaction of wild-type PTPRA with RET kinase-dead mutant, related to Figures 4A-B and 4D

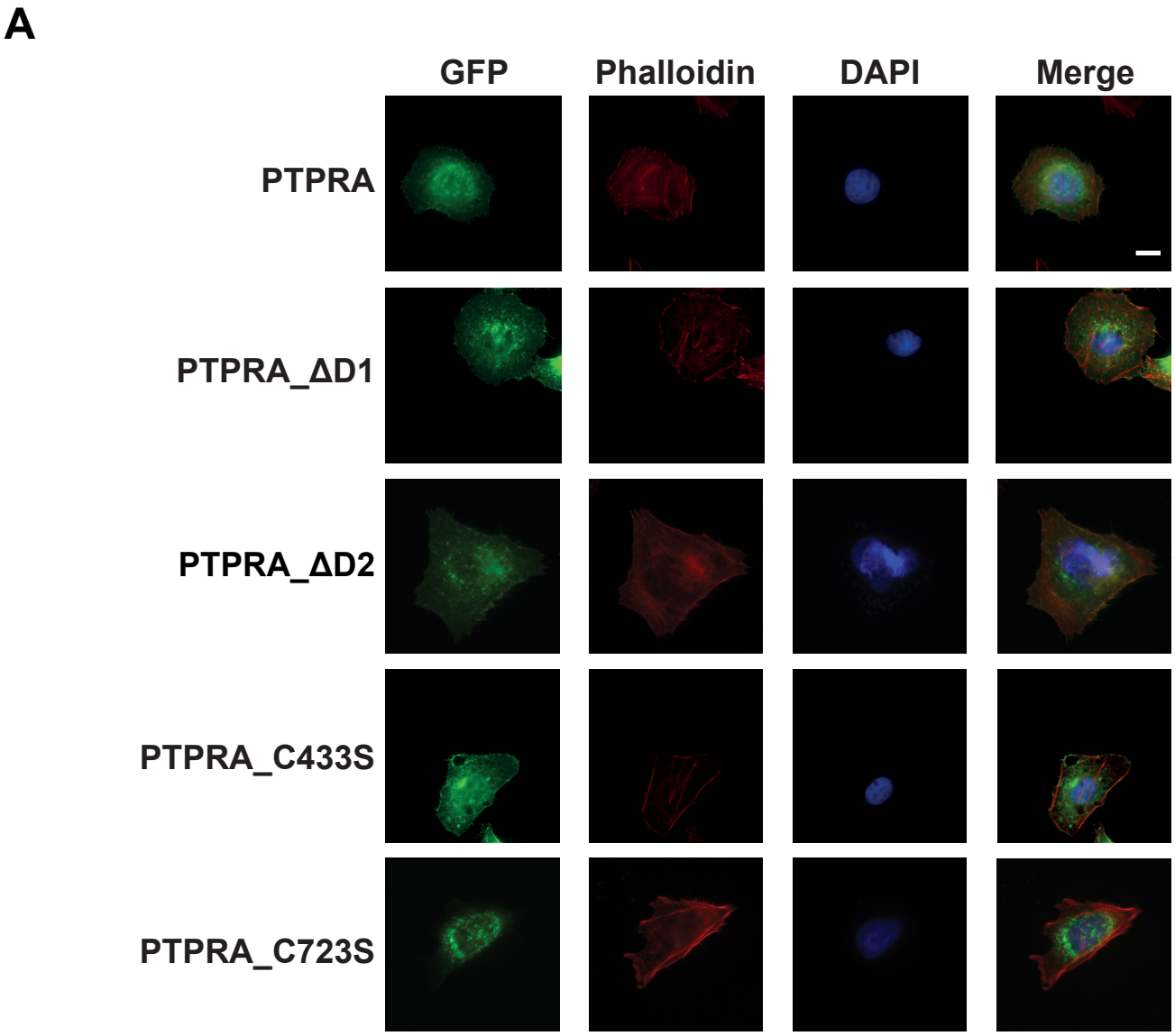

Figure S4. In vitro RET dephosphorylation coupled to mass spectrometry, related to Figure 5B

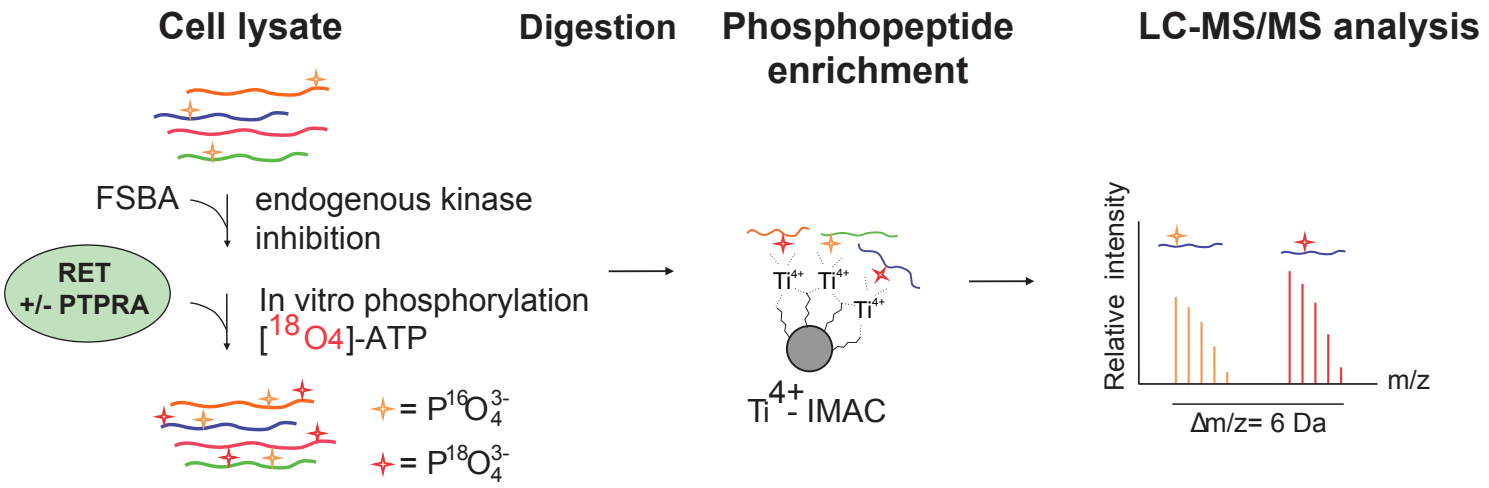

Figure S5. Colocalization of PTPRA with RET and MEN2 mutants, related to Figure 7A

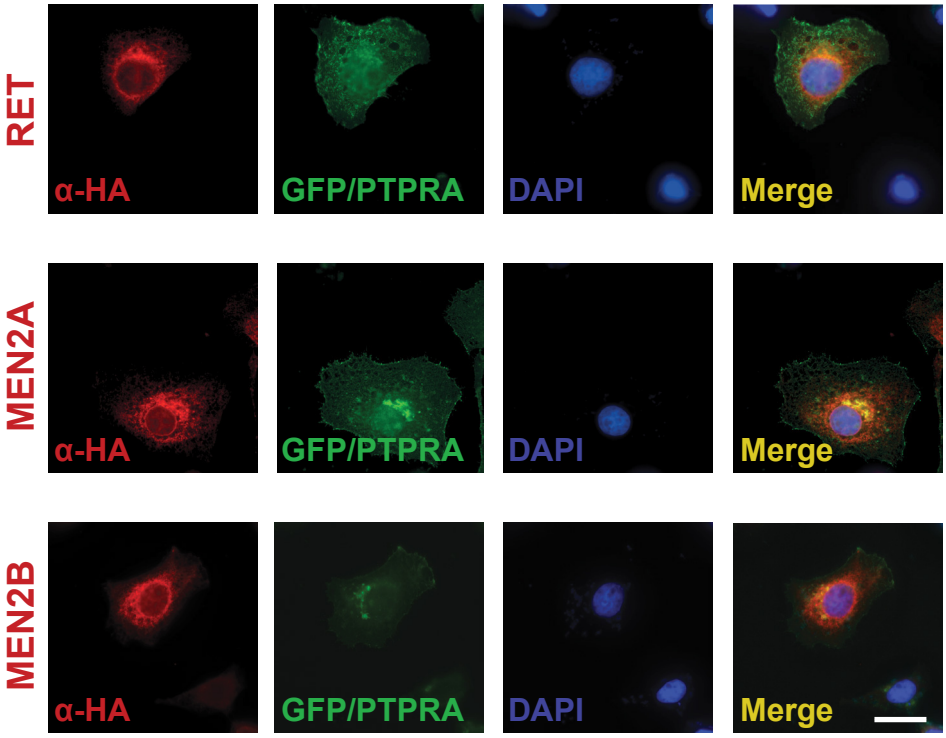

Supplemental Information

SUPPLEMENTAL FIGURE TITLES AND LEGENDS:

Figure S1. PTPRA and RET interactome overlap with EGFR, ERBB2, and IGF1R kinases, related to Figure 1B. The Venn diagram showing the proportion of common interactions between PTPRA, RET, EGFR, ERBB2, and IGF1R **(A and C)**. Also, shown are the number of shared interactions between the Ras-MAPK module and EGFR, ERBB2, and IGF1R kinases **(B)**. The inset shows the total number of (#) interactions identified with AP-MS and BioID methods for each bait.

Figure S2. Tissue-specific gene expression pattern of PTPRA, related to Figure 1. The box-plot indicates PTPRA gene expression (from Medisapiens) in healthy (green) and cancer (red) tissues. Similar tissues and cancers are grouped, with each having at least 5 samples. The bottom and top of the box are the 25^{th} and 75^{th} percentile of the data, respectively. The horizontal line is the median and whiskers extend to 1.5 times the interquartile range on both sides of the box. The outliers are shown as hollow circles. Expression levels (healthy and cancer) of PTPRA in specific- nervous, thyroid, pituitary, and kidney tissues are marked with arrowheads.

Figure S3. Expression of PTPRA mutants and interaction of wild-type PTPRA with RET kinase-dead mutant, related to Figures 4A-B and 4D. (A) HeLa cells were transfected with GFP-tagged wild-type or domain deletion (ΔD1 and ΔD2) mutant expression plasmids of PTPRA. The cells are stained with Alexa Fluor-594 phalloidin (red) and DAPI (blue) to visualize actin and nucleus, respectively. The scale bar for the immunofluorescence images is 10 μm. **(B)** HEK293-MSR cells were co-transfected

with StrepIII-HA-tagged wild-type PTPRA and then either with wild-type RET or RET kinase-dead (KD) mutant K758R (V5-tagged) expression constructs. The PTPRA significantly losses the interaction with RET KD mutant in comparison to wild-type RET. The immunoprecipitated (IP) proteins, as well as cell lysates, were immunoblotted with anti-V5 and anti-HA antibodies to detect RET and PTPRA proteins, respectively. Tubulin is used as a loading control.

Figure S4. *In vitro* RET dephosphorylation assay coupled to mass spectrometry, related to Figure 5B. HEK293 cell lysates (200 µg total protein) are treated with 5′-(4-fluorosulfonylbenzoyl)adenosine (FSBA) to inhibit endogenous kinases. Then, the lysate proteins are phosphorylated by incubating with recombinant RET or GFP (control) and γ-[$^{18}O_4$]-ATP (30°C for 30 min). After that, recombinant PTPRA is mixed for catalyzing dephosphorylation. The phosphopeptides from trypsin digested samples are enriched with Ti^{4+}-IMAC material and analyzed with LC-MS/MS.

Figure S5. Colocalization of PTPRA with RET and MEN2 mutants, related to Figure 7A. HeLa cells co-expressing GFP-tagged PTPRA with either StrepIII-HA-tagged RET or MEN2A or MEN2B constructs are stained with the anti-HA antibody. The nucleus is visualized with DAPI (blue) and co-localization is shown as yellow (scale bar = 10 µm).

TRANSPARENT METHODS

Experimental Model and Subject Details

The presented study utilized HEK293 (Human Embryonic Kidney; ATCC), HEK293-MSR (Invitrogen), HEK293 Flp-In T-Rex (Invitrogen), HeLa (Sigma), and MDCK (Madin-Darby Canine Kidney; ATCC) cell lines. MG87RET mouse fibroblast cells were a kind gift from Prof. Mart Saarma (Eketjall et al., 1999). All the cell lines were minimally cultured and routinely grown at 37°C and 5% CO2 in either Dulbecco Modified Eagle Medium (Sigma; HEK293, HEK293-MSR, HEK293 Flp-In T-Rex, and HeLa cells) or Minimum Essential Medium (Sigma; MDCK cells) supplemented with 100 µg/mL penicillin-streptomycin and 10% FBS or FCS (Sigma).

Expression plasmids

All cDNAs used in this study (PTPRA, RET, GDNF, and GRB2) were obtained from human ORFeome collection as Gateway-compatible entry vectors, where both wild-type PTPRA and RET (or RET9) plasmids correspond to their isoform 2 (793 and 1072 amino acids, respectively). PTPRA domain deletions (ΔD1: 1-231/492-793 amino acids and ΔD2: 1-523/783-793 amino acids), and point mutations (C433S, C723S, and Y789F), as well as RET point mutations (C634W; MEN2A, M918T; MEN2B, Y1062F, Y981F, and K758R), were created by Q5® Site-Directed Mutagenesis Kit (New England BioLabs, MA, USA) and confirmed by sequencing. They were inserted into following destinations vectors with C-terminal tags through LR recombination: pTO_StrepIII-HA_GW_FRT, pTO_StrepIII-HA-BirA_GW_FRT (MAC), pDest40_3xV5-6xHis_GW_FRT, and pTO_GFP fusion_GW_FRT (Liu et al., 2018, Yadav et al., 2017). All used constructs are made available via Addgene.org.

Cell Culture and transfections

HEK293, HEK293-MSR, HEK293 Flp-In T-Rex, HeLa, MDCK, and MG87RET cells were cultured in either Dulbecco Modified Eagle Medium (1000 mg/L glucose, L-glutamine; Sigma) or Minimum Essential Medium (Sigma) supplemented with 100 µg/mL penicillin-streptomycin and 10% FBS or FCS (Sigma). FuGENE® 6 (Promega; HEK293, HEK293-MSR, and HEK293 Flp-In T-Rex), FuGENE HD (Promega; MDCK), and HeLaFect (OZ Biosciences; HeLa) transfection reagents were used according to manufacturer's guidelines.

Protein complex purification

The stable HEK293 Flp-In T-Rex cell lines, inducibly expressing StrepIII-HA (AP-MS)- and StrepIII-HA-BirA (BioID)-tagged bait proteins: PTPRA, RET, GDNF, and GRB2, were prepared as described previously (Yadav et al., 2017). After 3 weeks of hygromycin B (Invitrogen) selection, cells were pelleted and subjected to single-step Strep affinity purifications under gentle (AP-MS) and harsh (BioID) lysis conditions, as previously reported (Liu et al., 2018; Yadav et al., 2017). The eluted complex proteins were trypsin (Promega) digested (overnight at 37°C) to short peptides and were cleaned with C-18 microspin columns (The Nest Group Inc. USA) as per manufacturer's instructions.

Liquid chromatography-mass spectrometry (LC-MS/MS) and data analysis

The LC-MS/MS analysis of the peptide sample, in four replicates, was accomplished on EASY-nLC II- system coupled to Q Exactive™ Hybrid Quadrupole-Orbitrap Mass Spectrometer (Thermo Fisher Scientific). An 80-minute linear gradient from 5 to 35%

of buffer B (98% ACN and 0.1% FA) at a flow rate of 300 nl/min was run for peptide separation under similar m/z and resolution settings applied before (Yadav et al., 2017). The MS spectral files were extracted with PD version 1.4 (Thermo Fisher Scientific) for protein identification using the UniProtKB database (human, release version 2018/08) at false discovery rate (FDR) of 0.05. Other database search parameters were used as previously (Yadav et al., 2017).

Luciferase-reporter assay

HEK293 or MG87RET cells, at density of 1.5 x 10^4 cells/well, were plated in white clear-bottom 96-well assay plates (Corning® 3610) and were transfected with 45 ng pStrepIII-HA-RET (wild-type or MEN2 mutants) and 9 ng pGBD-Elk 1 plasmids along with 45 ng Firefly pGAD-FR-Luc and 2 ng Renilla phR-Luc luciferase-reporter plasmids per well. The Strep-HA-tagged (pStrepIII-HA) versions of both PTPRA (WT or domain deletion or CS or YF point mutants) and GFP (green fluorescent protein from Jellyfish) expression vectors were also transfected either as 50 ng or in a range of 0-50 ng. The next day, the cells were co-stimulated with soluble GDNF (100 ng/mL; R & D Systems) and GFRα1 (500 ng/mL; R & D Systems) complex for 24 h. Post-treatment, they were lysed in 1x passive lysis buffer and the luciferase-reporter activity from 5 replicates was measured using the Dual-Luciferase® Reporter Assay System (Promega) on ClarioSTAR (BMG Labtech) multilabel-microplate reader. The experiments were always repeated two times.

Co-immunoprecipitation

HEK293-MSR cells (~5 x 10^5 cells) were seeded in 6-well plates and transiently transfected with StrepIII-HA- and V5-tagged expression constructs of the indicted

protein of interest. Subsequently, after 24 h, they were lysed in buffer: 50 mM HEPES pH 8.0, 5 mM EDTA, 150 mM NaCl, 50 mM NaF, 0.5 % NP40, 1 mM DTT, 1.5 mM Na3VO4, 1 mM PMSF, supplemented with 1x protease inhibitors cocktail (Sigma). One-tenth of clear cell lysate was saved and remaining was immunoprecipitated with anti-HA agarose beads slurry (mouse monoclonal; Sigma) for 4 h at 4°C. The immunocomplexes and cell lysates were finally suspended in 2x Laemmli's buffer.

Western blot analysis

Heat-denatured immunoprecipitated samples and lysates were resolved on precast SDS-PAGE gels (any-kDa Mini-PROTEAN; Bio-Rad) and transferred onto a nitrocellulose membrane (Whatman GmbH) with semi-dry electro-blotting apparatus (Bio-Rad). The membranes were blocked with either 5% non-fat milk or 5% BSA in TBS-T (1x TBS-0.05% Tween-20) and were probed with appropriate primary antibodies (mouse monoclonal): anti-V5 (1:5000; Thermo Fisher Scientific), anti-HA.11 (1:2000; BioLegend), anti-pTyr (1:2000; clone 4G10; Millipore), and anti-alpha tubulin (1:10,000; Abcam) as well as rabbit polyclonal p44/42 MAPK (T202/Y204; 1:1000; Cell Signaling Technology). Either anti-mouse (1:2000; GE Healthcare) or anti-rabbit (1:2000; Dako) horseradish peroxidase conjugated secondary antibodies were used and bands were visualized with Amersham ECL detection system (GE Healthcare) on photographic film (Fujifilm). For reprobing, blots were incubated in stripping buffer (RestoreTM PLUS, Thermo Fisher Scientific) for 15 min at room temperature.

Fluorescent microscopy

HeLa cells were grown on fibronectin-coated coverslips in 4-well plates and transfected (HeLaFect) with either wild-type or domain deleted (ΔD1 and ΔD2) or CS point mutants of PTPRA (GFP-tagged) expression constructs. StrepIII-HA-tagged wild-type RET or MEN2A or MEN2B plasmids are also co-transfected, wherever applicable. Then, 24 h later, standard steps of fixation, permeabilization, and blocking were carried out as previously reported (Yadav et al., 2017). To visualize the RET, cells were incubated with anti-HA.11 primary followed by Alexa Fluor-594 (goat anti-mouse; Thermo Fisher Scientific) conjugated secondary antibodies. The actin and nucleus were labeled with Alexa Fluor-594 phalloidin (Thermo Fisher Scientific) and 4′,6-diamidino-2-phenylidole (DAPI; Sigma), respectively. The coverslips were mounted with Mowiol embedding media (Merck) and imaged under the Leica DM5000B microscope with a 63x/1.40-0.60 HCX PL APO oil objective. All images were processed with ImageJ software (https://imagej.nih.gov/).

PTPRA phosphatase assay

2 μg of recombinant RET (Thermo Fisher Scientific) was suspended in PTP buffer (25 mM Tris-HCl, pH 7.0, 50 mM NaCl, 2 mM EDTA, and 2 mM DTT). About 4 μg of recombinant GFP (Novus Biologicals) or PTPRA phosphatase (Sigma) was mixed and dephosphorylation was carried out at 30°C for 30 min. The sample was divided into two and the reaction was stopped by either 5x Laemmli's buffer (for immunoblotting) or 8 M urea (for LC-MS/MS analysis). Standard steps of immunoblotting using anti-pTyr primary antibody were performed as described above. The LC-MS/MS analysis was conducted as described above and MS-raw data was searched with MaxQuant version 1.6.0.16 (Andromeda search engine) for phosphopeptide quantification using the human UniProtKB release version 2017/12 (20192 entries) (Cox and Mann, 2008).

MS-based *in vitro* RET dephosphorylation assay

HEK293 cells were lysed (50 mM Tris-HCl, pH 7.5, 150 mM NaCl, 5 mM EDTA, 1% NP-40, and protease inhibitors cocktail; Sigma) and protein content was measured using BCA protein assay kit (Thermo Fisher Scientific). About 200 µg of total protein was reacted with 1 mM 5′-(4-fluorosulfonylbenzoyl)adenosine (FSBA; Sigma) and 10% DMSO in Tris-HCl, pH 7.5 at 30°C (1 h) for inhibition of endogenous kinases. Excess FSBA was removed and the buffer was changed to kinase assay buffer (50 mM Tris-HCl, pH 7.5, 10 mM MgCl2, 1 mM DTT) using Amicon Ultra-4 centrifugal filter units (10 kDa cut-off, Millipore). For kinase reaction, samples were incubated with 300 ng recombinant RET (Thermo Fisher Scientific) or GFP (Novus Biologicals) and 1 mM γ-[18O4]-ATP (Cambridge Isotope Laboratory) at 30°C for 30 min. Then for dephosphorylation, 600 ng recombinant PTPRA phosphatase (Sigma) or GFP were added and incubated for another 1 h. The reaction was stopped by 8 M urea. The MS sample preparation steps (reduction, alkylation, trypsinization, and C-18 desalting) were conducted as described earlier (Yadav et al., 2017). Next, Ti4+-IMAC phosphopeptide enrichment was conducted as reported previously (Zhou et al., 2013). In short, Ti4+-IMAC beads were loaded onto GELoader tips (Thermo Fisher Scientific) and conditioned with loading buffer (80% acetonitrile; ACN, 6% trifluoroacetic acid; TFA). The protein digests were dissolved in loading buffer and added into the spin tips. The columns were washed first with 50% ACN, 0.1% TFA with 200 mM NaCl and then without salt. The bound phosphopeptides were eluted with 10% ammonia, followed by C-18 purification before LC-MS analysis on Q Exactive™ Hybrid Quadrupole-Orbitrap Mass Spectrometer (settings in Yadav et al., 2017).

For phosphopeptide quantification, the MS raw data was searched with MaxQuant version 1.6.0.16 (Andromeda search engine) (Cox and Mann, 2008) using the human UniProtKB release version 2017/12 (20192 entries). Search criteria from Yadav et al., 2017 were utilized, except additional heavy phosphorylation of serine/threonine/tyrosine (+85.966 Da) was employed as the dynamic modification.

3D type I collagen invasion assay

MDCK cells were transiently transfected (FuGENE HD) with StrepIII-HA-tagged RET, MEN2A, MEN2B, PTPRA expression vectors. The 3D collagen invasion assay was prepared as previously described (Sugiyama et al., 2013). Briefly, cell culture inserts in 24-well plates were overlaid with rat tail collagen I (2.2 mg/mL; Sigma) and transfected MDCK cells, suspended in MEM, were added on top (3×10^5 cells/insert). Medium supplemented with GDNF-GFRα1 (50 ng-250 ng) as chemoattractants was added to the lower chamber of 3D collagen gels. After the cells have grown for 7 days, the inserts were fixed with 4% PFA and embedded into paraffin. Hematoxylin and eosin-stained sections were imaged under the DM6000B microscope (Leica).

Quantification and Statistical Analysis

The MS-interactome data from four replicates was filtered against GFP controls. The preys appearing in all replicates with frequency ≤ 3 and average PSM < 1.5 were excluded. Preys obtained in either AP-MS or BioID purifications and showing average PSM fold-change (avg. GFP/avg. prey) of at least > 1.5 are retained for interactome. For luciferase assay, replicate-averaged data (n=5 replicates) from two independent experiments was used and fold-changes under different conditions were calculated as RET+GFP vs. RET+PTPRA in either absence or presence of ligand when applicable.

The error bars represent either standard deviation or standard error of the mean (SEM). p-values (indicated by asterisks) were obtained by a two-tailed Student´s t-test, where statistical significance is expressed as follows: $p < 0.0001$ (***) and $p < 0.001$ (**). The heat-map was based on log2 of raw MS-intensities under RET+GFP vs. RET+PTPRA experimental set-up. However, for pTyr-phosphorylation bar graphs the % phosphorylation change is obtained as RET+PTPRA vs. RET+GFP, where the phosphorylation in RET+GFP control sample (i.e. maximum) is set to 100%.

Bioinformatics processing

The network of filtered preys was constructed with Cytoscape 3.1.0 (http://www.cytoscape.org/) (Shannon et al., 2003). The known, novel, and prey-to-prey interactions were retrieved from the Protein Interaction Network Analysis (PINA v2.0) database (http://cbg.garvan.unsw.edu.au/pina/). The PTPRA gene expression profile was extracted from IST Online (Medisapiens; http://ist.medisapiens.com/). Heat-map and MS-based protein localization polar maps were generated by Morpheus (https://software.broadinstitute.org/morpheus/) and Mass Spectrometry (MS)-Microscopy (https://msmicroscopy.shinyapps.io/msmic/) online tools, respectively. The relative intensity of the tyrosine-phosphorylated RET band was quantified with ImageJ (https://imagej.nih.gov/).

SUPPLEMENTAL REFERENCES:

Cox, J., and Mann, M. (2008). MaxQuant enables high peptide identification rates, individualized p.p.b.-range mass accuracies and proteome-wide protein quantification. *Nat Biotechnol* 26**,** 1367-72.

Shannon, P., Markiel, A., Ozier, O., Baliga, N.S., Wang, J.T., Ramage, D., Amin, N., Schwikowski, B., and Ideker, T. (2003). Cytoscape: a software environment for integrated models of biomolecular interaction networks. *Genome Res* 13**,** 2498-504.

Sugiyama, N., Gucciardo, E., Tatti, O., Varjosalo, M., Hyytiainen, M., Gstaiger, M., and Lehti, K. (2013). EphA2 cleavage by MT1-MMP triggers single cancer cell invasion via homotypic cell repulsion. *J Cell Biol* 201**,** 467-84.

Zhou, H., Ye, M., Dong, J., Corradini, E., Cristobal, A., Heck, A.J., Zou, H., and Mohammed, S. (2013). Robust phosphoproteome enrichment using monodisperse microsphere-based immobilized titanium (IV) ion affinity chromatography. *Nat Protoc* 8**,** 461-80.